Landau–Zener–Stückelberg interferometry

S.N. Shevchenko [a,b,*], S. Ashhab [b,c], Franco Nori [b,c]

[a] *B.Verkin Institute for Low Temperature Physics and Engineering, Kharkov, Ukraine*
[b] *RIKEN Advanced Science Institute, Wako-shi, Saitama, Japan*
[c] *Department of Physics, The University of Michigan, Ann Arbor, MI, USA*

A R T I C L E   I N F O

A B S T R A C T

A transition between energy levels at an avoided crossing is known as a Landau–Zener transition. When a two-level system (TLS) is subject to periodic driving with sufficiently large amplitude, a sequence of transitions occurs. The phase accumulated between transitions (commonly known as the Stückelberg phase) may result in constructive or destructive interference. Accordingly, the physical observables of the system exhibit periodic dependence on the various system parameters. This phenomenon is often referred to as Landau–Zener–Stückelberg (LZS) interferometry. Phenomena related to LZS interferometry occur in a variety of physical systems. In particular, recent experiments on LZS interferometry in superconducting TLSs (qubits) have demonstrated the potential for using this kind of interferometry as an effective tool for obtaining the parameters characterizing the TLS as well as its interaction with the control fields and with the environment. Furthermore, strong driving could allow for fast and reliable control of the quantum system. Here we review recent experimental results on LZS interferometry, and we present related theory.

Contents

* Corresponding author at: B.Verkin Institute for Low Temperature Physics and Engineering, Kharkov, Ukraine.
  E-mail address: sshevchenko@ilt.kharkov.ua (S.N. Shevchenko).

1. Introduction

1.1. Strongly driven TLSs: a brief historical review

The model of a quantum two-level system (TLS), with only two relevant quantum states, is used to describe a variety of physical systems. At first, it was used in relation to spins and atomic collisions, which describe natural microscopic systems. It has been used to describe various other naturally occurring settings ever since. Furthermore, some artificial mesoscopic systems that were realized recently in semiconductor quantum dots and superconducting circuits can operate as effective TLSs. These solid-state TLSs have received increasing attention recently for two main reasons: they exhibit fundamental quantum phenomena on macroscopic scales, and they are considered possible candidates to operate as quantum bits (qubits) in future quantum information processing devices.

It is quite common that the two energy levels of a quantum TLS exhibit an *avoided level crossing* or anticrossing as some external parameter is varied, as shown in Fig. 1. The physical properties of the two energy eigenstates are typically exchanged when going from one side of the avoided crossing to the other side. If the external control parameter is varied in time such that the system traverses the avoided crossing region, a non-adiabatic transition between the two energy levels can occur. The transition probability is usually named after Landau and Zener (LZ) in recognition of their pioneering work on this subject, Landau (1932b) and Zener (1932).

If a LZ transition is one step in a sequence of coherent processes occurring during the dynamics, not only the change in the occupation probabilities but also the change in the relative *phase* between the quantum states is relevant. In particular, in this review we shall focus on the situation where the control parameter is varied periodically and strongly, such that the system keeps going back and forth across the avoided crossing region. In this case, the physical observables exhibit periodic dependence on the phase acquired between the transitions (Stückelberg, 1932; Landau, 1932a). This periodicity, which is the basis of Landau–Zener–Stückelberg (LZS) interferometry, provides a useful tool that allows the characterization of the parameters defining the quantum TLS and its interaction with the control fields and the environment. We note here that the formula for the single-passage transition probability can also be found in the paper Majorana (1932), and it can alternatively be named the Landau–Zener–Stückelberg–Majorana formula, as proposed in Di Giacomo and Nikitin (2005).

1.1.1. Atomic physics

The problem of strongly driven TLSs appears in a number of contexts in atomic physics. In atomic-collision problems, the electronic state of the atom pair can experience a LZ transition from the ground states of the incoming atoms into a hybridized intermediate state and then back to the electronic ground states of the outgoing atoms. In this case the avoided crossing region is passed twice (Child, 1974; Nikitin and Umanskii, 1984), and the Stückelberg phase typically has large variations and hence its interferometric consequences are washed out (Stückelberg, 1932; Landau, 1932a).

An atom in an intense laser field can also experience LZ transitions, but in contrast to atomic-collision problems, the atom is driven periodically in time and multiple LZ transitions occur (Delone and Krainov, 1985). In the case of an atom in a laser field, (regardless of the field intensity) if the atom is driven at a frequency that matches its energy-level splitting, it can be resonantly excited to an upper level. Then, at low driving amplitudes, the level occupation probabilities experience Rabi oscillations (Rabi, 1937). When the driving amplitude is increased, multiphoton processes become relevant. These processes occur when the energy-level splitting matches the energy of an integer number of photons (Shirley, 1965). These multiphoton processes have traditionally been described by making use of Floquet theory [(Autler and Townes, 1955; Ritus, 1967; Sambe, 1973; Zel'dovich, 1973; Barone et al., 1977; Aravind and Hirschfelder, 1984); for a review see Chu and Tel'nov (2004)]. In addition to controlling atomic states, resonant driving of atoms has also been studied as a means for finding atomic parameters, and the parameters of quantum systems in general (Coffey et al., 1969; Henry and Lang, 1977).
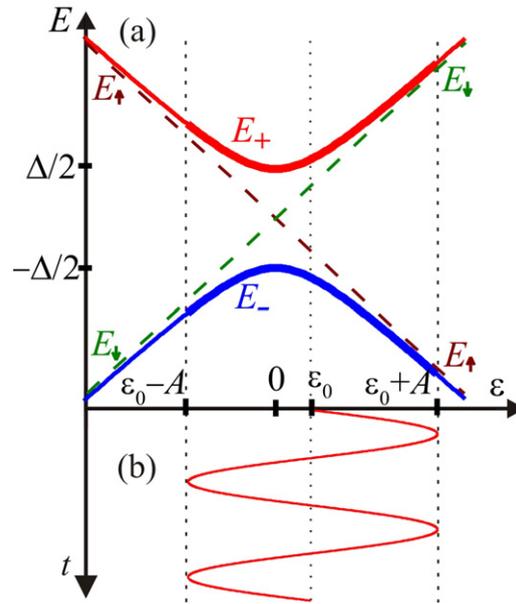
Fig. 1. (Color online) (a) Energy levels E versus the bias ε. The two solid curves (red and blue) represent the *adiabatic energy levels*, $E_\pm$, which display avoided crossing with energy splitting Δ. The dashed lines show the crossing *diabatic energy levels* $E_{\uparrow,\downarrow}$, corresponding to the diabatic states $\varphi_\uparrow$ and $\varphi_\downarrow$. (b) The bias ε represents the driving signal, and it oscillates between $\varepsilon_{\min} = \varepsilon_0 - A$ and $\varepsilon_{\max} = \varepsilon_0 + A$ with a sinusoidal time dependence: $\varepsilon(t) = \varepsilon_0 + A \sin \omega t$.

1.1.2. Other systems

In addition to atomic systems, LZS interference has been studied in a number of other systems. (Related discussions of the intracycle and intercycle interference were given in Ashhab et al. (2007) and Arbo et al. (2010). For example, periodic dependence and time-domain oscillations related to LZS interference have been predicted in the electronic transport in semiconductor superlattices (Rotvig et al., 1995, 1996). Stückelberg oscillations were also studied in superconducting quantum point contacts biased with a dc voltage and exposed to periodic driving (Gorelik et al., 1998). This effect was proposed as a sensitive tool for microwave-photon detection. Another example of interference in microscopic systems arises in the study of interacting magnetic molecules (Wernsdorfer et al., 2000; Garanin, 2004), molecular nanomagnets (Calero et al., 2005; Földi et al., 2007, 2008), and single nitrogen vacancy centers in diamond (Fuchs et al., 2009). Interference effects have also been predicted to take place in the interlayer tunneling in quasi-one-dimensional layered materials, such as organic conductors (Cooper and Yakovenko, 2006; Banerjee and Yakovenko, 2008), and in the tunneling of a periodically driven two-mode Bose–Einstein condensate (Zhang et al., 2008a,b). Recently, LZ tunneling and Stückelberg oscillations were measured in a gas of ultracold molecules (Mark et al., 2007a,b) and in the dipole–dipole interaction between Rydberg atoms (van Ditzhuijzen et al., 2009).

Avoided level crossings can also be used in the study of second-order phase transition problems (Damski and Zurek, 2006; Dziarmaga, 2009). Periodic driving around a phase transition can then result in interference fringes (Mukherjee and Dutta, 2009). The LZS model has also been used to describe the singlet-triplet transition for the state of two electrons in a semiconductor double quantum dot (Ribeiro and Burkard, 2009; Petta et al., 2010; Burkard, 2010; Ribeiro et al., 2010) as well as the transport of photons between two halves of an optical cavity divided by a dielectric membrane (Heinrich et al., 2010). Recent technological advances have also allowed the realization of the strong-driving regime in superconducting qubits, where such interference has been observed in several experiments (Oliver et al., 2005; Sillanpää et al., 2006; Wilson et al., 2007; Izmalkov et al., 2008; Sun et al., 2009; LaHaye et al., 2009). Such superconducting qubit systems will be discussed in more detail below.

1.1.3. Theory of LZS interferometry

The theory of driven quantum TLSs has been studied in numerous papers [for reviews see Leggett et al. (1987), Grifoni and Hänggi (1998), Thorwart et al. (2001), Vitanov et al. (2001), Zhu et al. (2001) and Frasca (2003)]. Some of the recent work has focused on the impact of the environment, e.g. Ao and Rammer (1991), Thorwart et al. (2000), Wubs et al. (2006), Zueco et al. (2008) and Nalbach and Thorwart (2009). In particular, some papers pointed out that if the relaxation in the system is small enough, interference between multiple LZ transitions becomes relevant for the system's dynamics, e.g. Shimshoni and Gefen (1991), Saito and Kayanuma (2002) and Saito et al. (2007); when the avoided crossing is passed several times, interference can take place and the dynamics is sensitive to the phase acquired between successive crossings, e.g. Kayanuma (1994).

LZS interference has also been recently proposed as a possible approach to achieve perfect population transfers and to implement quantum gates for quantum-control and quantum-computing purposes (Teranishi and Nakamura, 1998; Zhu et al., 2001; Gaitan, 2003; Zwanziger et al., 2003; Nagaya et al., 2007; Li et al., 2009) [related work on combining adiabatic

LZ crossings with coherent dynamics can be found in Goswami (2003), Vitanov et al. (2003), Kral et al. (2007), Oh et al. (2008) and Wei et al. (2008)].

The purpose of the present review is to present the theory of strongly driven TLSs and LZS interferometry and recent experimental results on the subject, particularly in relation to superconducting qubits.

1.2. Superconducting qubits

Superconducting qubits are Josephson-junction-based circuits that can behave as effective two-level systems. There are several types of superconducting qubits, differing mostly by their topology and by their physical parameters. They are generally called phase, charge, or flux qubits. For reviews see Makhlin et al. (2001), Devoret and Martinis (2004), You and Nori (2005), Wendin and Shumeiko (2007), Zagoskin and Blais (2007) and Clarke and Wilhelm (2008).

Superconducting qubits have several properties that make them unique for studying quantum effects. The qubits have mesoscopic size, which means that they allow the observation of quantum effects on a macroscopic scale. They can be integrated in electrical circuits, which provides different ways of controlling and probing their states. Their parameters are adjustable: they can be tuned by changing the applied bias current, gate voltage, or magnetic flux. The qubit's state can be probed by measuring the charge or current induced in it. These unique properties of superconducting qubits allow the realization of the strong-driving regime, and they have allowed the realization of several experiments on LZS interferometry in the past few years.

1.3. Fano and Fabry–Perot interferometry using superconducting qubits

Superconducting qubits can be used for LZS interferometry, but also to study other types of interferometry, including Fano and Fabry–Perot interferometry (Zhou et al., 2008a,b; Liao et al., 2010). These latter devices can be implemented using quasi-one-dimensional open systems where photons are injected from the left and move towards the right side of the device. Along the way, the photons interact with either one or two qubits acting as tunable mirrors, controlled by changing the applied electric and/or magnetic fields on the qubits. These qubits, working as tunable mirrors, can change the reflection and transmission coefficients of the photons confined in waveguides.

Let us first consider the case of a single superconducting qubit interacting with an incoming photon (Zhou et al., 2008a). When the energy of the incoming photon matches the energy spacing of the qubit, the photon is reflected, otherwise it is transmitted. This type of single-photon switch exhibits Breit–Wigner scattering: now in one dimension instead of the standard three dimensional case for natural atoms. This Breit–Wigner scattering produces a symmetric Lorentzian peak in the reflection coefficient, versus frequency, of the photon. This situation occurs when the dispersion relation of the incoming photon is linear, as in a transmission line resonator, acting as a "rail" guiding the motion of the photons. When the photon dispersion relation is nonlinear, for long-wavelength photons propagating in a quasi-one-dimensional array of coupled cavities, the reflection coefficient exhibits an asymmetric Fano line shape, due to the interference between the continuous mode of the incoming photon and the discrete energy levels of the qubit. Thus, for single-photon transport in a one-dimensional waveguide, the photons can be partially or totally reflected by a controllable two-level system which can act as a tunable mirror.

It is known that the Fabry–Perot interferometer, which consists of two highly reflecting planar mirrors, provides the simplest cavity. It is then natural to ask the question: "is it possible to construct a quantum version of a Fabry–Perot interferometer?" Namely, to build a resonator, in a one-dimensional waveguide, with two tunable-mirrors made of quantum scatterers. Reference (Zhou et al., 2008b) focused on this question and studied quantum analogs of the Fabry–Perot interferometer. They found that two separate two-level systems interacting with photons in a waveguide can also create, between them, single-photon quasi-bound states. A recent work (Liao et al., 2010) studied a more complex form of interferometry, with the goal of controlling the transport of single photons by tuning the frequency of either one or two cavities in an array of coupled cavities guiding the 1D motion of photons. In some regimes, the photons can be localized around the scatterers, which act as impurities, producing isolated states in the gap of the energy spectrum (Zhou et al., 2008b; Liao et al., 2010).

1.4. Hamiltonian and bases

The main subject of this review is a strongly and periodically driven TLS. A quantum TLS with energy bias ε and tunneling amplitude Δ is described by the Hamiltonian

$$H(t) = -\frac{\Delta}{2}\sigma_x - \frac{\varepsilon(t)}{2}\sigma_z \tag{1}$$

in terms of the Pauli matrices $\sigma_{x,z}$ ($\hbar = 1$ is assumed throughout). One generally thinks of Δ as being fixed by the system properties, and ε as being a tunable control parameter; hence ε is a function of time t and Δ is not. We assume the monochromatic time-dependent bias

$$\varepsilon(t) = \varepsilon_0 + A \sin \omega t, \tag{2}$$

with amplitude A, frequency ω and offset ε_0.

Note that this problem with the time-dependent component along the z-axis can be related to the one with the time-dependent component along the x-axis by a $\pi/2$-rotation around the y-axis:

$$H'(t) = e^{-i\frac{\pi}{4}\sigma_y} H(t) e^{i\frac{\pi}{4}\sigma_y} = -\frac{\Delta}{2}\sigma_z + \frac{\varepsilon(t)}{2}\sigma_x. \tag{3}$$

The latter Hamiltonian is typical for problems such as an atom in a laser field. It should also be noted that having different signs in the Hamiltonian than the ones given above does not cause any nontrivial change in the results.

The instantaneous eigenvalues of $H(t)$ depend on the bias $\varepsilon(t)$ as follows:

$$E_{\pm}(t) = \pm\frac{1}{2}\Omega(t), \tag{4}$$

$$\Omega(t) = \sqrt{\Delta^2 + \varepsilon(t)^2}. \tag{5}$$

The ε-dependence of the energy levels is shown in Fig. 1. In particular, it shows an avoided level crossing at $\varepsilon = 0$.

Although the TLS is a rather simple-looking model, concrete calculations on it can present significant difficulties. Specifically, the Schrödinger equation can be written as a second-order differential equation with periodic coefficients, the Hill equation, which is not solvable in analytic closed form (Grifoni and Hänggi, 1998). Nevertheless, different theoretical approaches can be used to obtain approximate analytical results in various parameter regions.

As we shall explain in detail below, one key relation for purposes of deciding the suitability of a given theoretical approach is that between the driving frequency ω and the minimal energy splitting Δ. In superconducting qubits, both limits, $\omega \ll \Delta$ (Sillanpää et al., 2006) and $\omega \gg \Delta$ (Oliver et al., 2005), have been realized in recent experiments. Another key relation concerns the velocity of passing the avoided level region, which is of the order of $A\omega$ (we also introduce the adiabaticity parameter δ later in Eqs. (19) and (20)). We will distinguish between the slow driving regime, $A\omega \lesssim \Delta^2$, and the fast driving regime, $A\omega \gg \Delta^2$. The natural representations for the two regimes are formulated in the adiabatic and diabatic bases, respectively. The *diabatic basis* $\{\varphi_{\uparrow}, \varphi_{\downarrow}\}$ is formed with the eigenstates of σ_z: $\sigma_z\varphi_{\uparrow} = \varphi_{\uparrow}$, $\sigma_z\varphi_{\downarrow} = -\varphi_{\downarrow}$ (note that these states would be the eigenstates of the Hamiltonian if Δ vanished). The *adiabatic basis* consists of the instantaneous eigenstates of the time-dependent Hamiltonian: $H(t)\varphi_{\pm}(t) = E_{\pm}(t)\varphi_{\pm}(t)$. The two bases are related to each other by the time-dependent coefficients $\beta_{\pm}(t)$ (see Appendix A for details):

$$\varphi_{\pm}(t) = \beta_{\mp}(t)\varphi_{\uparrow} \mp \beta_{\pm}(t)\varphi_{\downarrow}, \tag{6}$$

$$\beta_{\pm}(t) = \sqrt{\frac{\Omega(t) \pm \varepsilon(t)}{2\Omega(t)}}. \tag{7}$$

Any given wave function of the quantum TLS can be decomposed in either one of these two bases; the coefficients in the quantum superposition are the probability amplitudes for the respective states.

2. Theory: adiabatic-impulse model

There are a number of theoretical approaches that can be used to study the problem of a strongly driven TLS. Among these approaches, the adiabatic-impulse model, which we shall explain in detail below (and in Appendices A and B), is perhaps the most intuitive whenever the TLS is repeatedly driven through the avoided crossing. We shall therefore put special emphasis on this theoretical approach in this review. Three alternative theoretical approaches, which in certain parameter regimes can be well suited for the study of this problem, will be discussed in Appendices C (rotating-wave approximation), D (Floquet theory) and E (dressed-state picture).

The adiabatic energy levels $E_{\pm}$ introduced in Section 1.3 have a minimum distance of Δ, and this minimum distance is realized at times $t_{1,2} + 2\pi n/\omega$, where $\omega t_1 = \arcsin(-\varepsilon_0/A)$ and $\omega t_2 = \pi - \omega t_1$, see Fig. 2; here n is an integer. Because the energy eigenstates, i.e. the states of the adiabatic basis, change rather rapidly around the avoided-crossing region and are approximately constant far to the right or far to the left of that region, one would intuitively expect that the system will evolve almost adiabatically far from the points of avoided crossing and the evolution becomes nonadiabatic in the vicinity of these points. One could therefore make the approximation that beyond a certain boundary the evolution is completely adiabatic. However, it is convenient not to introduce an arbitrary boundary between the adiabatic and nonadiabatic regions and instead consider the evolution to be adiabatic everywhere except at the points of minimum energy separation, where the system experiences a sudden mixing in the populations of the two energy levels. Naturally, these sudden transitions do not occur in reality. However, provided that the system follows a linear ramp traversing the avoided crossing region, one can still obtain an accurate description of the net result of the adiabatic and nonadiabatic parts of the evolution. This discretized picture only simplifies the algebra that arises in the relevant calculations. The calculation presented in Appendix A can be used to obtain the appropriate assignment for the adiabatic phases and the mixing matrices at the crossing points in order to obtain the correct expressions describing the system's dynamics. Following Damski and Zurek (2006) (see also Zurek (1996) and Damski (2005)) we call this picture the adiabatic-impulse approximation to emphasize the two-stage character of the model. In particular, this name emphasizes that the non-adiabatic transitions are described as instantaneous, which is just
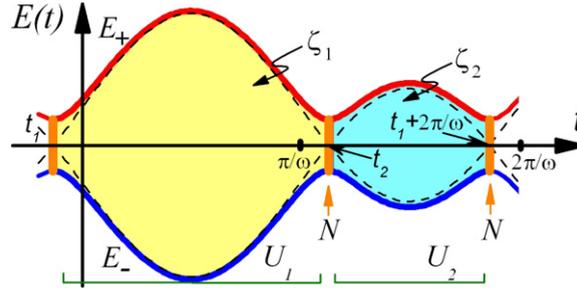
Fig. 2. (Color online) Time evolution of the energy levels during one period. The time-dependent adiabatic energy levels define a two-stage evolution: transitions at the non-adiabatic regions, described by the evolution matrix N, and the adiabatic evolution, described by the matrices $U_{1,2} = \exp(-i\zeta_{1,2}\sigma_z)$. The acquired phases $\zeta_{1,2}$ have a geometrical interpretation: they are equal to the area under the curves, shown by the yellow and blue regions. The diabatic energy levels, $\pm\varepsilon(t)/2$, are shown by the dashed lines.

a convenient description of the continuous dynamics; see also original articles, where the adiabatic-impulse theory was developed (Delone and Krainov, 1985; Averbukh and Perel'man, 1985; Vitanov and Garraway, 1996; Garraway and Vitanov, 1997; Damski and Zurek, 2006)].

2.1. Adiabatic evolution

The wave function $\psi(t)$ that describes the quantum state of the TLS as a function of time can be decomposed in the adiabatic basis (see Appendix A):

$$\psi(t) = \sum_{\pm} b_{\pm}(t)\varphi_{\pm}(t) = \sum_{\pm} c_{\pm}(t)\varphi_{\pm}(t) \exp\left\{\mp i\left(\zeta + \frac{\pi}{4}\right)\right\}, \tag{8}$$

$$\zeta = \frac{1}{2}\int \Omega(t)\mathrm{d}t. \tag{9}$$

Since in the adiabatic approximation $c_{\pm}$ are time-independent coefficients between crossings, the adiabatic evolution from $t = t_i$ to $t = t_f$ (assuming that no LZ transitions are encountered) can be described by the evolution matrix U, defined as follows

$$\mathbf{b}(t_f) = U(t_f, t_i)\mathbf{b}(t_i), \tag{10}$$

$$\mathbf{b}(t) \equiv \begin{pmatrix} b_+ \\ b_- \end{pmatrix}, \tag{11}$$

$$U(t_f, t_i) = \begin{pmatrix} e^{-i\zeta(t_f, t_i)} & 0 \\ 0 & e^{i\zeta(t_f, t_i)} \end{pmatrix} = e^{-i\zeta(t_f, t_i)\sigma_z}, \tag{12}$$

$$\zeta(t_f, t_i) = \frac{1}{2}\int_{t_i}^{t_f} \Omega(t)\mathrm{d}t. \tag{13}$$

In particular, the phases acquired during the adiabatic stages (see Fig. 2) are given by:

$$\zeta_1 = \frac{1}{2}\int_{t_1}^{t_2} \Omega(t)\mathrm{d}t, \quad \zeta_2 = \frac{1}{2}\int_{t_2}^{t_1+2\pi/\omega} \Omega(t)\mathrm{d}t. \tag{14}$$

2.2. Single passage: Landau–Zener transition

Consider the nonadiabatic region in the vicinity of $t_{1,2}$: $t = t_{1,2} + t'$, $\omega |t'| \ll 1$. Then the bias can be linearized:

$$\varepsilon(t_{1,2} + t') \approx \pm vt', \tag{15}$$

where

$$v = A\omega |\cos \omega t_{1,2}| = A\omega\sqrt{1 - \left(\frac{\varepsilon_0}{A}\right)^2}. \tag{16}$$

The linearized Hamiltonian

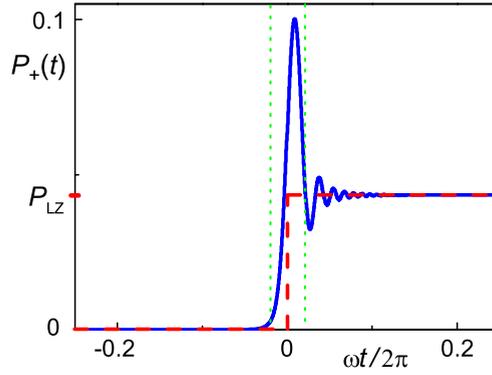$$H(t') = -\frac{\Delta}{2}\sigma_x \mp \frac{vt'}{2}\sigma_z \tag{17}$$

Fig. 3. (Color online) One-passage LZ transition. The time dependence of the upper level occupation probability $P_+(t)$ is plotted for the following parameters: $A/\Delta = 10$, $\omega/\Delta = 0.05$, $\varepsilon_0 = 0$. The blue solid curve presents the exact numerical solution, while red dashed curve corresponds to the analytical solution. The time interval between the vertical green dotted lines corresponds to the crossover region, which is characterized by t_{LZ}.

is exactly that of the LZ problem. The solution of the LZ problem in terms of the parabolic cylinder function is presented in detail in Appendix A. For discussions of different theoretical approaches to the LZ problem, see e.g. Delos and Thorson (1972), Benderskii et al. (2003) and Wittig (2005). Here, in the main text, we also present the shortest solution, based on the fact that the transition under the adiabatic perturbation has quasiclassical character, where the change of the action (given by the integral $\int E(t)dt$) is large (Landau and Lifshitz, 1977). Then the problem of the transition under the adiabatic perturbation is formally fully analogous to the problem of the quasiclassical over-barrier reflection.

　　Assuming that the system is initially in the lower energy level, the transition probability from the lower to the upper level during the single-sweep process is described within the quasiclassical approximation as follows (Landau and Lifshitz, 1977). The energy levels coincide at two points in the complex plane: at $t' = \pm t_0 = \pm i\Delta/v$ one finds that $E_+(t_0) = E_-(t_0)$. Accordingly, the probability P_+ that the system ends up in the upper level is determined by the contour integral in the plane of complex time:

$$P_+ = \exp\left(-2\mathrm{Im}\int_0^{t_0}[E_+(t') - E_-(t')]dt'\right). \tag{18}$$

Calculating this integral for $2E_\pm = \pm\sqrt{\Delta^2 + (vt')^2}$ and $t_0 = i\Delta/v$, we obtain the LZ transition probability:

$$P_+ = P_{LZ} = \exp\left(-2\pi\delta\right), \tag{19}$$

$$\delta = \frac{\Delta^2}{4v}. \tag{20}$$

Eq. (19) describes the transition probability for an arbitrary value of the exponent (Nikitin, 1996). As the driving velocity v is changed from 0 (adiabatic limit) to ∞ (sudden-change limit), the transition probability P_+ varies from zero to unity. In Fig. 3 the red dashed curve shows the instantaneous transition of the adiabatic-impulse model, with the mixing probability given by Eq. (19). The blue solid curve is calculated numerically by integrating the Schrödinger equation (Shevchenko et al., 2005). Note that the LZ formula (19) accurately describes the final upper level occupation probability P_+, but it does not describe the transient dynamics in the vicinity of the energy-level avoided crossing. This issue was studied in detail in Refs. Mullen et al. (1989), Vitanov (1999) and Zenesini et al. (2009). In particular, it was shown that the duration of the transition (the region between the green dotted lines in Fig. 3) can be estimated as follows:

$$t_{LZ} \sim \frac{2}{\Delta}\sqrt{\delta}\max(1, \sqrt{\delta}). \tag{21}$$

Here we would like to note that, as argued in Garraway and Vitanov (1997), Eq. (21) gives only the upper limit of the transition time, and one can think of the transition time is being shorter than the one given in Eq. (21). The conditions of the applicability of the adiabatic-impulse model, which describes the LZS interferometry, require that the relations Δ/ω and/or A/ω are large (Garraway and Vitanov, 1997):

$$\Delta^2 + A^2 \gg \omega^2. \tag{22}$$

In particular, the multiphoton fringes were shown to be described by this model at $A \lesssim \omega \lesssim \Delta$ in Krainov and Yakovlev (1980).

　　The LZ formula (19) describes the upper level occupation probability P_+, which is the square of the absolute value of the probability amplitude. However, when interference is relevant (as will be discussed in detail below), one has also to know the change in the relative phase between the two components of the wave function as the crossing region is traversed. One
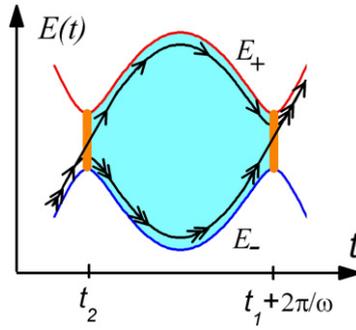
Fig. 4. (Color online) Double-passage transition. Adiabatic energy levels as in Fig. 2 are plotted. The lines with one and two arrows show the two trajectories where the transition to the upper level happens during the first and the second passages of the avoided level crossing. Their respective transition probabilities are given by $P_{LZ}(1 - P_{LZ})$ and $(1 - P_{LZ})P_{LZ}$, while the interference is described by Eq. (27).

can keep track of this phase by describing the LZ transition using the (non-adiabatic) unitary evolution matrix N, which is derived in Appendix A:

$$\mathbf{b}(t_{1,2} + 0) = N\mathbf{b}(t_{1,2} - 0), \tag{23}$$

$$N = \begin{pmatrix} \sqrt{1 - P_{LZ}}\, e^{-i\widetilde{\varphi}_S} & -\sqrt{P_{LZ}} \\ \sqrt{P_{LZ}} & \sqrt{1 - P_{LZ}}\, e^{i\widetilde{\varphi}_S} \end{pmatrix}, \tag{24}$$

$$\widetilde{\varphi}_S = \varphi_S - \frac{\pi}{2}, \tag{25}$$

$$\varphi_S = \frac{\pi}{4} + \delta(\ln \delta - 1) + \arg \Gamma(1 - i\delta), \tag{26}$$

where φ_S is the so-called Stokes phase (see e.g. Child (1974), Kayanuma (1997) and Wubs et al. (2005)) and Γ is the gamma function.

2.3. Double passage: Stückelberg phase

Consider now the double-passage process, where the avoided crossing region is passed twice at the same speed. This double-passage problem corresponds to one full driving cycle of the periodic driving that we are considering. The probability for the upper level P_+ after one period is given by Eq. (B.5) with $n = 1$:

$$P_+ = 4P_{LZ}(1 - P_{LZ}) \sin^2 \Phi_{St}, \tag{27}$$

$$\Phi_{St} = \zeta_2 + \widetilde{\varphi}_S. \tag{28}$$

This result, that the probability of excitation P_+ is an oscillating function of a certain phase Φ_{St}, was first obtained in (Landau, 1932a; Stückelberg, 1932). The Stückelberg phase Φ_{St} consists of two components: the first ζ_2 is acquired during the adiabatic evolution and the second $\widetilde{\varphi}_S$ during the non-adiabatic transitions.

Stückelberg oscillations were observed in atomic inelastic scattering cross-sections (Nikitin and Ovchinnikova, 1972) and in the microwave excitation of Rydberg atoms (Baruch and Gallagher, 1992; Yoakum et al., 1992). However, in many cases these Stückelberg oscillations average out and can be neglected, and one only needs to consider the averaged probability (Nikitin, 1996)

$$\overline{P_+} = 2P_{LZ}(1 - P_{LZ}). \tag{29}$$

The above expression is the sum of two probabilities, which correspond to the system being excited at the first or at the second passage through the avoided-crossing region. These two components are schematically illustrated in Fig. 4 with trajectories marked by single and double arrows, respectively.

The quantum-mechanical interference between the different LZ transitions has the result that the net excitation probability after the double passage can range from 0 (destructive interference) to $4P_{LZ}(1 - P_{LZ})$ (constructive interference) according to Eq. (27). The latter probability is twice as large as the one without interference, Eq. (29). This situation is analogous to the one encountered in the Mach–Zehnder interferometer (Ji et al., 2003; Oliver et al., 2005; Pezze et al., 2007).

2.4. Multiple passage

Let us now study a multiple-passage process, where the system passes the avoided-crossing region periodically. Consider first the relevant time scales. The characteristic time for an LZ transition t_{LZ} can be estimated from Eq. (21). The time between
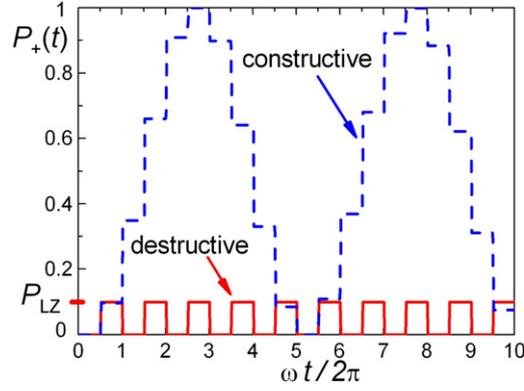
Fig. 5. (Color online) Constructive (blue dashed line) versus destructive (red continuous line) interference. Time dependence of the upper level occupation probability P_+ with constructive ($\zeta_1 = \pi/2 + k\pi$) and destructive ($\zeta_1 = k\pi$) interference at $\varepsilon_0 = 0$ and $P_{LZ} = 0.1$. The TLS is taken to be initially in the lower level.

subsequent tunneling events is of the order of half driving period $T/2 = \pi/\omega$. LZS interference takes place when (i) successive LZ transitions events do not overlap and (ii) the phase coherence (characterized by the dephasing time T_2) is preserved:

$$t_{LZ} < T/2 < T_2. \tag{30}$$

In this subsection we assume $T/2 \ll T_2$ and ignore decoherence. For definiteness, as the initial condition we consider the system to be in the ground state at time $t_1 + 0$. Then the state at time t, after n full periods, is described by the following evolution matrices (see Fig. 2):

$$U\left(t, t_1 + \frac{2\pi n}{\omega}\right)(NU_2NU_1)^n \quad \text{for } t - \frac{2\pi n}{\omega} \in (t_1, t_2), \tag{31}$$

$$U\left(t, t_2 + \frac{2\pi n}{\omega}\right)NU_1(NU_2NU_1)^n \quad \text{for } t - \frac{2\pi n}{\omega} \in \left(t_2, t_1 + \frac{2\pi}{\omega}\right), \tag{32}$$

$$U_{1,2} = \exp(-i\zeta_{1,2}\sigma_z). \tag{33}$$

One can now derive expressions for the evolution matrices in terms of the parameters in the Hamiltonian (1), as explained in Appendix B. Using these matrices one can analyze the dynamics for any given initial state. Fig. 5 illustrates two different possibilities that correspond to constructive and destructive interference between consecutive crossings.[1] In addition to the time dependence, one can also derive expressions for the average populations of the two quantum states as functions of the system parameters, since it is common to experimentally measure the steady-state populations of these states. In general, one needs to make approximations in order to obtain clear analytical results. Below we consider two opposite limits, depending on whether the individual crossings are slow (i.e., almost adiabatic) or fast (i.e., almost sudden). As explained in Appendix B (see also Ashhab et al. (2007)), in both cases a resonance condition can be derived that determines whether the system will exhibit oscillations between the two basis states. This condition is given by

$$(1 - P_{LZ}) \sin \zeta_+ - P_{LZ} \sin \zeta_- = 0, \tag{34}$$

where

$$\zeta_+ = \zeta_1 + \zeta_2 + 2\widetilde{\varphi}_S, \tag{35}$$
$$\zeta_- = \zeta_1 - \zeta_2. \tag{36}$$

As we shall see shortly, this resonance condition results in drastically different patterns in the slow- and fast-passage limits.

2.4.1. Slow-passage limit

In the limit $\delta \gg 1$, $P_{LZ} \ll 1$ and the resonance condition reduces to

$$\zeta_+ = \zeta_1 + \zeta_2 + 2\widetilde{\varphi}_S = k\pi, \tag{37}$$

for any integer k, and $\widetilde{\varphi}_S \approx -\pi/2$. Going further and deriving an analytic expression in terms of Δ, ε_0 and A is complicated by the fact that the integrals that determine ζ_1 and ζ_2 cannot be evaluated in closed analytic form. Numerical calculations,

---

[1] These cases are also clearly illustrated in the two computer animations available online at http://dml.riken.jp/animations.php.
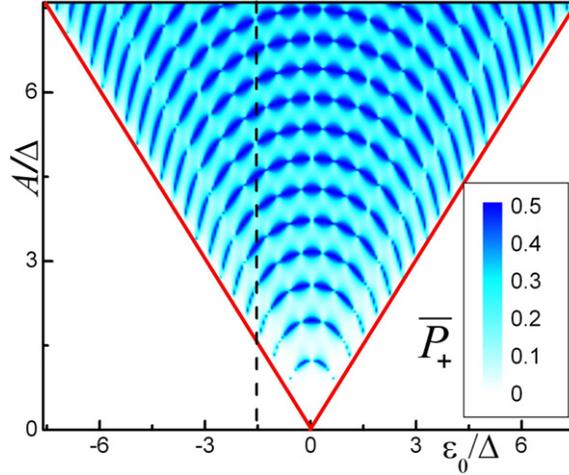
Fig. 6. (Color online) Slow-driving LZS interferometry for $A\omega \lesssim \Delta^2$. The time averaged upper level occupation probability $\overline{P_+}$ as a function of the energy bias ε_0 and the driving amplitude A. The graph is calculated with Eq. (38) for $\omega/\Delta = 0.32 < 1$. The inclined red lines mark the region of the validity of the theory: $\varepsilon_0 < A$, which means that the system experiences avoided level crossings. Outside of this region the excitation probability is negligibly small. The vertical dashed line shows the alteration of the excitation maxima and minima.

Table 1

Parameters used in different experiments studying LZS interferometry: tunneling amplitude Δ, maximal driving amplitude A^{max}, and driving frequency ω in the units GHz$\times 2\pi$, minimal adiabaticity parameter $\delta^{min} = \Delta^2/(4\omega A^{max})$, and maximal LZ probability $P_{LZ}^{max} = \exp(-2\pi\delta^{min})$.

	Δ	A^{max}	ω	δ^{min}	P_{LZ}^{max}
(Oliver et al., 2005)	0.004	24	1.2	10^{-7}	1
(Sillanpää et al., 2006)	12.5	95	4	0.1	0.5
(Wilson et al., 2007)	2.6	62	7	0.004	0.98
(Izmalkov et al., 2008)	3.5	40	4	0.02	0.9

however, are straightforward. The resonance condition (37) describes arcs around the point $A = \varepsilon_0 = 0$ (see Fig. 6), where we treat Δ as a fixed parameter. Taking the system to be initially in the lower energy level, the average occupation probability of the upper level is given by (see Eq. (B.13) in Appendix B):

$$\overline{P_+} = \frac{P_{LZ}(1 + \cos\zeta_+ \cos\zeta_-)}{\sin^2\zeta_+ + 2P_{LZ}(1 + \cos\zeta_+ \cos\zeta_-)}. \tag{38}$$

From this expression one can see that on resonance (i.e., when $\sin\zeta_+ = 0$) the upper level occupation probability is maximal, $\overline{P_+} = 1/2$. One can also see that the widths of the resonance lines are modulated by the numerator in Eq. (38); it tends to zero at points where

$$\cos\zeta_+ \cos\zeta_- = -1. \tag{39}$$

Fig. 6 illustrates the interferometric pattern obtained from Eq. (38). In this figure we use the parameters of (Sillanpää et al., 2006) (see also Table 1). Note that for any value of the energy bias offset ε_0, the maxima and minima alternate with increasing driving amplitude A (see the color variation along the vertical dashed line in Fig. 6), as was studied by Shytov et al. (2003) and Shevchenko et al. (2005).

In the case of zero offset $\varepsilon_0 = 0$, one can go a little bit further with the analytic derivation. Taking $\varepsilon_0 = 0$ we have $\zeta_1 + \zeta_2 \approx 2A/\omega$ and $\zeta_1 - \zeta_2 = 0$ and the resonance condition (Eq. (37)) is satisfied when

$$2A/\omega = k\pi. \tag{40}$$

One can alternatively analyze the dynamics in the time domain. When $\varepsilon_0 = 0$, $t_1 = 0$ and $t_2 = \pi/\omega$, and from Eq. (B.5) in the first approximation in P_{LZ} it follows that

$$P_+(t) = P_{LZ}\frac{\sin^2 n\phi}{\sin^2 \phi} \equiv \frac{P_{LZ}}{\cos^2\zeta_1 + P_{LZ}\sin^2\zeta_1}\sin^2 n\phi, \tag{41}$$

$$\zeta_1 = \frac{1}{2}\int_0^{\pi/\omega} \Omega(t)\mathrm{d}t = \frac{\sqrt{\Delta^2 + A^2}}{\omega}\widetilde{E}\left(\frac{A}{\sqrt{\Delta^2 + A^2}}\right), \tag{42}$$

where $\widetilde{E}(x)$ is the full elliptic integral of the second kind.

Let us now analyze the expression for $P_+(t)$, Eq. (41). The prefactor of $\sin^2 n\phi$ has a minimum at $\zeta_1 = k\pi$ (where this prefactor is equal to P_{LZ}) and a maximum at $\zeta_1 = \frac{\pi}{2} + k\pi$ (where it is equal to 1). Thus, the former case ($\zeta_1 = k\pi$) corresponds to destructive interference and the latter case ($\zeta_1 = \frac{\pi}{2} + k\pi$) corresponds to constructive interference. These two cases are illustrated in Fig. 5. Note that the latter case corresponds to the coherent destruction of tunneling, which has been studied extensively in the literature (Grossmann et al., 1991a,b; Grossmann and Hänggi, 1992; Kayanuma and Saito, 2008; Eckel et al., 2009; Ho et al., 2009; Wubs, 2010). From Eq. (41) for the cases of constructive and destructive interference we obtain:

$$\text{constructive: } P_+(t) = \sin^2\left(\sqrt{P_{LZ}}\, n\right), \quad \zeta_1 = \frac{\pi}{2} + k\pi, \tag{43}$$

$$\text{destructive: } P_+(t) = P_{LZ} \sin^2\left(\frac{\pi}{2}n\right), \quad \zeta_1 = k\pi. \tag{44}$$

The dynamics (i.e., the time dependence of P_+) in the cases of constructive and destructive interference is illustrated in Fig. 5. The resonance condition $\zeta_1 = \frac{\pi}{2} + k\pi$ with Eq. (42) in the limit of strong driving (i.e., $A \gg \Delta$) takes the form (Shevchenko and Omelyanchouk, 2006):

$$2A/\omega = \pi(2k+1). \tag{45}$$

The positions of the resonances depend on the ratio A/ω but not on Δ, as was studied in detail by Shytov et al. (2003). Note that Eq. (40) predicts more resonance peaks than Eq. (45). The explanation of this discrepancy is that at $\varepsilon_0 = 0$ and for even values of k the resonance peaks of Eq. (40) disappear according to Eq. (39), and we recover Eq. (45). Interestingly, if we take Eq. (42) in the limit of weak driving (i.e., $A \ll \Delta$), we obtain:

$$\Delta = (2k+1)\omega.$$

This relation describes the odd multiphoton resonances, as studied by Shirley (1965) and Krainov and Yakovlev (1980), where the energy level separation Δ is an odd multiple of a photon energy ω. We have therefore obtained the correct resonance condition, even though the weak-driving limit is outside the regime of validity of the above derivation, which is based on the interference of multiple LZ crossings.

2.4.2. Fast-passage limit

In the limit $\delta \ll 1$, $(1 - P_{LZ}) \ll 1$ and the resonance condition reduces to

$$\zeta_- = \zeta_1 - \zeta_2 = k\pi. \tag{46}$$

Unlike the slow-passage limit, one can now derive an approximate analytic expression for $\zeta_1 - \zeta_2$ in the large-amplitude limit (the reason is that the parts of the yellow and blue areas in Fig. 2 that are difficult to calculate cancel when taking the difference between the two areas):

$$\zeta_- = \zeta_1 - \zeta_2 \approx \frac{1}{2}\int_{t_1}^{t_1 + 2\pi/\omega} (\varepsilon_0 + A\sin\omega t)\, \mathrm{d}t = \frac{\pi\varepsilon_0}{\omega}. \tag{47}$$

The resonance condition is therefore given simply by

$$\varepsilon_0 = k\omega. \tag{48}$$

If the system is driven on resonance (with a given value k), and taking the TLS to be initially in the lower diabatic state (i.e., $\varphi_\uparrow$ or $\varphi_\downarrow$ depending on the sign of ε_0), the system exhibits full oscillations between $\varphi_\uparrow$ and $\varphi_\downarrow$:

$$P_{up}^{(k)}(t) = \frac{1}{2}\left(1 - \cos\Omega_R^{(k)}t\right). \tag{49}$$

The oscillation frequency can be calculated from the effective rotation angle in the full-cycle evolution matrix (NU_2NU_1), as was done in (Ashhab et al., 2007). In the limit $A \gg \varepsilon_0$ we find that

$$\Omega_R^{(k)} \approx \Delta\sqrt{\frac{2\omega}{\pi A}}\left|\cos\left(\frac{A}{\omega} - k\frac{\pi}{2} - \frac{\pi}{4}\right)\right|. \tag{50}$$

As in the slow-passage limit, the Rabi frequency exhibits periodic behavior in the fast-passage limit as well. In particular, it vanishes whenever the cosine function in Eq. (50) vanishes. The interferometric pattern that results in this case is shown in Fig. 7.

Above we have used the adiabatic-impulse approach to analyze the response of the TLS to the driving field. To demonstrate another approach, next we consider the results of the rotating-wave approximation (RWA); for more details see Appendix C.
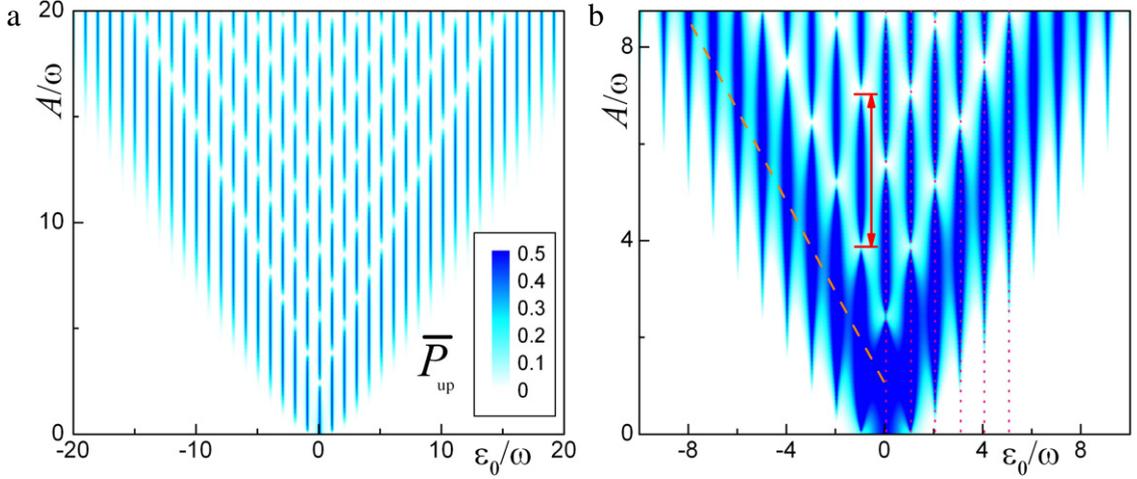
Fig. 7. (Color online) Fast-driving LZS interferometry for $A\omega \gg \Delta^2$: dependence of the time-averaged upper diabatic state occupation probability $\overline{P}_{up}$ on ε_0/ω and A/ω. The graphs are plotted using Eq. (57) for $\omega/\Delta = 300 \gg 1$, $\omega T_1/(2\pi) = 2.4 \times 10^4$ and $\omega T_2/(2\pi) = 24$ (a) and $\omega/\Delta = 1.14 > 1$, $\omega T_1/(2\pi) = \omega T_2/(2\pi) = 6$ (b). Several multiphoton resonances are shown by the vertical pink dotted lines at $\varepsilon_0 = k\omega$ (for $k = 0, 1, 2, \ldots, 5$, only) modulated by Bessel functions. The vertical red double-arrow in (b) shows the distance between two consecutive zeros of the Bessel function.

If decoherence processes are not taken into account, the TLS is described by the Schrödinger equation. Its solution gives the probability of the upper diabatic state P_{up}, which exhibits k-photon Rabi oscillations:

$$P_{up}^{(k)}(t) = \frac{\Delta_k^2}{2\Omega_R^{(k)2}} \left(1 - \cos \Omega_R^{(k)} t\right), \tag{51}$$

$$\Delta_k = \Delta J_k\left(\frac{A}{\omega}\right), \tag{52}$$

$$\Omega_R^{(k)} = \sqrt{(k\omega - \varepsilon_0)^2 + \Delta_k^2}, \tag{53}$$

where J_k is the Bessel function. Note that the k-photon Rabi frequency is described by a power law at small driving, $A/\omega \ll 1$; namely, at $\varepsilon_0 = k\omega$:

$$\Omega_R^{(k)} = \Delta_k \approx \frac{\Delta}{k!} \left(\frac{A}{2\omega}\right)^k. \tag{54}$$

Changing the system parameters (ε_0 or ω), we pass through different k-photon resonances. Thus, the time-averaged probability $\overline{P}_{up}$ can be described by the sum of the Lorentzian-shape k-photon resonances:

$$\overline{P}_{up} = \sum_k \overline{P}_{up}^{(k)} = \frac{1}{2} \sum_k \frac{\Delta_k^2}{(k\omega - \varepsilon_0)^2 + \Delta_k^2}. \tag{55}$$

The position of the resonances is (quasi-) periodic in the parameters ε_0, ω^{-1}, A; this corresponds to the multiphoton relation $\varepsilon_0 = k\omega$ and to the quasi-periodic character of the Bessel functions $J_k(A/\omega)$ for large value of the argument:

$$J_k\left(\frac{A}{\omega}\right) \approx \sqrt{\frac{2\omega}{\pi A}} \cos\left(\frac{A}{\omega} - \frac{\pi}{4}(2k + 1)\right). \tag{56}$$

Note that the oscillations described by Eq. (56) represent the counterpart to the Stückelberg oscillations of the double-passage problem (Nikitin, 1996).

Note here that the results derived in the adiabatic-impulse approach and those of the RWA are essentially the same. These results can also be derived using Floquet theory (Son et al., 2009) (see also Appendix D) or using the dressed-state picture, which represent the hybridization of the qubit and photon degrees of freedom (Liu et al., 2006; Wilson et al., 2007) (see also Appendix E).

Relaxation can be described using the Bloch equations for the reduced density matrix; the influence of the environment is taken into account using the phenomenological energy and phase relaxation times, T_1 and T_2. In Appendix C we obtain the stationary solution of the Bloch equations, which at zero temperature results in the excitation probability:

$$\overline{P}_{up} = \frac{1}{2} \sum_k \frac{\Delta_k^2}{\frac{1}{T_1 T_2} + \frac{T_2}{T_1}(k\omega - \varepsilon_0)^2 + \Delta_k^2}. \tag{57}$$
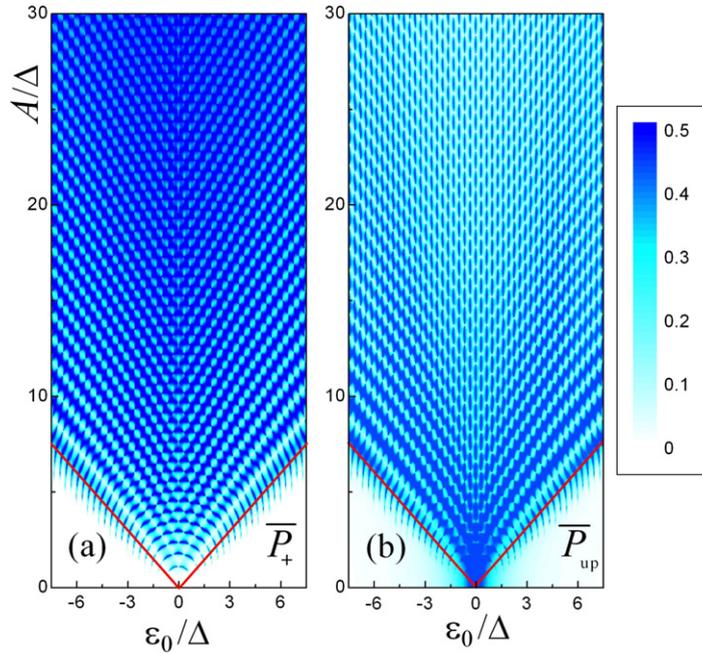
Fig. 8. (Color online) Crossover from the slow-passage limit (bottom part of the figure) to the fast-passage limit (top part of the figure) as the driving amplitude A is increased. On the left the steady-state probability $\overline{P}_+$ of the *adiabatic* excited state is plotted as a function of bias offset ε_0 and driving amplitude A. On the right the probability $\overline{P}_{\text{up}}$ of the upper *diabatic* state is plotted. One can see that the resonance features are clearest in the adiabatic basis for slow passage and in the diabatic basis for fast passage. The ratio ω/Δ is equal to 0.32, and there is no decoherence. Note that panel (a) differs from Fig. 6 because that figure was generated using Eq. (38), whereas in this figure we numerically solve the Bloch equations.

In the limit where the dephasing and relaxation times are large and equal to each other, i.e., $T_1 = T_2 \to \infty$, the above expression (somewhat accidentally) coincides with the time averaged solution of the Schrödinger equation, Eq. (55). In Fig. 7 we plot the probability $\overline{P}_{\text{up}}$ with Eq. (57) for the parameters of Refs. Oliver et al. (2005) and Izmalkov et al. (2008) (see Table 1).

We emphasize here that the distinction between the interference patterns in Figs. 6 and 7 is determined not by the ratio ω/Δ, but rather by the ratio $\omega\sqrt{A^2 - \varepsilon_0^2}/\Delta^2$. This point is illustrated in Fig. 8, where one can see the crossover from the slow-passage to the fast-passage limit as the driving amplitude A is increased. Note that in order to see this crossover for a fixed frequency, one needs to take a small value of ω/Δ.

The analysis of the positions of the multiphoton resonances allows to do spectroscopy and to obtain the parameters of the TLS. To calibrate the power of the generator one can use the distance between the minima or maxima in the Stückelberg oscillations (one of them is shown in Fig. 7 with the vertical red double-arrow), or alternatively, the slope of the interference fringes (shown by the orange dashed line in Fig. 7). The analysis of the interference fringes also allows to obtain the parameters that characterize the relaxation of the system due to the interaction with the environment. This was theoretically discussed in Shytov et al. (2003) and experimentally realized in Oliver et al. (2005), Sillanpää et al. (2006), Wilson et al. (2007) and Izmalkov et al. (2008). The longitudinal T_1 and transverse T_2 relaxation times can be extracted from the shapes of the resonances in Eq. (57). Moreover the effective temperature can be estimated using Eqs. (C.15) and (C.16) from the shape of the first resonance, where $\Delta E \approx |\varepsilon_0| \approx \omega$ which is typically of the order of 1 GHz and smaller for superconducting TLSs.

In practice it can be useful to perform more detailed calculations beyond the stationary solution in Eq. (57). We note that the relaxation times, T_1 and T_2, can be introduced phenomenologically as two fitting parameters (as in Oliver et al. (2005)) or calculated within certain model for dissipating environment (as in Sillanpää et al. (2006)). For superconducting qubits a convenient model is the spin-boson model, which models the environment as a bath of harmonic oscillators (Makhlin et al., 2001; Wendin and Shumeiko, 2007; McDermott, 2009; Wilson et al., 2010); in this model both T_1 and T_2 are parameter-dependent and determined by the strength of dissipation. However in many cases the relaxation can be described by effective parameter-independent times T_1 and T_2; in this paper for plotting Fig. 7 we have taken the relaxation times, T_1 and T_2, for simplicity being constant. Also, the Bloch equations (C.13) can be solved exactly as, e.g., in Shevchenko et al. (2008), which allows one to relax the assumption $\Delta \ll \omega$; the positions of the multiphoton resonances are then defined by the relation: $\Delta E \approx \sqrt{\Delta^2 + \varepsilon_0^2} \approx k\omega$. Note that the inhomogeneity of the field due to low-frequency noise cannot be directly described within the Bloch equations (Abragam, 1961); it results in the broadening of the Lorentzian-shaped resonances and can be described as the additional term in the expression for the width of the resonances, as in Ref. Oliver et al. (2005).
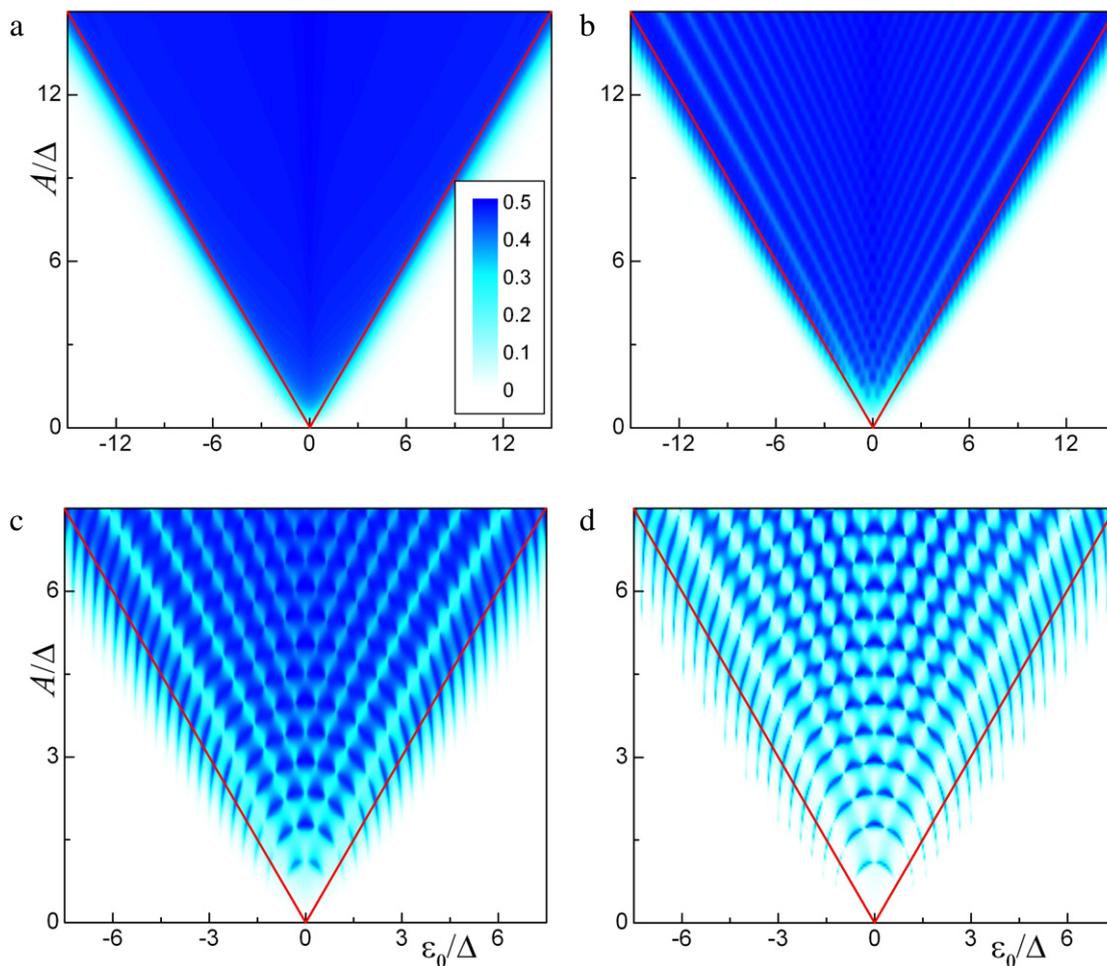
Fig. 9. (Color online) Same as in Fig. 6 (i.e. LZS interferometry with low-frequency driving), but including the effects of decoherence. The time averaged upper level occupation probability $\overline{P_+}$ was obtained numerically from the Bloch equations with the Hamiltonian (1). The dephasing time T_2 is given by $\omega T_2/(2\pi) = 0.1$ in (a), 1 in (b), 5 in (c) and $T_2 = 2T_1$ in (d). The relaxation time is given by $\omega T_1/(2\pi) = 10$.

2.5. Decoherence

When studying the effect of decoherence on the dynamics of a quantum system, it is perhaps most common to start from the case of zero decoherence and slowly increase the decoherence rates. In the problem of LZS interferometry, we find it simpler to think about the effect of *coherence* rather than the effect of decoherence. We study the effect of coherence by considering the steady-state populations of the two quantum states of the TLS (as was done in Berns et al. (2006)). We note here that in the slow-passage limit we analyze the populations of the adiabatic-basis states whereas in the fast-passage limit we analyze the populations of the diabatic-basis states.

Starting from the limit of strong decoherence, no interference between the different LZ transitions occurs. The result is then simple. If the driving amplitude is large enough to take the TLS through the avoided crossing, each crossing will act as a small "kick" to the populations of the two states, and these kicks will eventually add up such that the TLS reaches a steady state with equal population of the two energy levels (the ground state can have a higher population if relaxation is substantial). If the driving amplitude A is smaller than the bias offset $|\varepsilon_0|$, no LZ transitions will occur, and the system will remain in the lower level. This situation is depicted in Figs. 9(a) and 10(a).

We now increase the coherence time such that the two transitions in a single driving period are separated by a time that is smaller than the coherence time. The transitions induced by different driving cycles are separated by more than the coherence time, and they therefore act as independent kicks. As in the case of strong decoherence, a sufficiently large amplitude is required to drive transitions between the two quantum states. However, if the phase accumulated between the two interfering transitions corresponds to destructive interference, the net effect of a full driving period will be no mixing at all. As a result, we now find lines in the A–ε_0 plane where the TLS is driven back and forth across the avoided crossing but the system remains in the lower level (in the fast-passage limit, the TLS remains in the diabatic state that corresponds to the lower level for the given value of ε_0). This situation is depicted in Figs. 9(b) and 10(b).
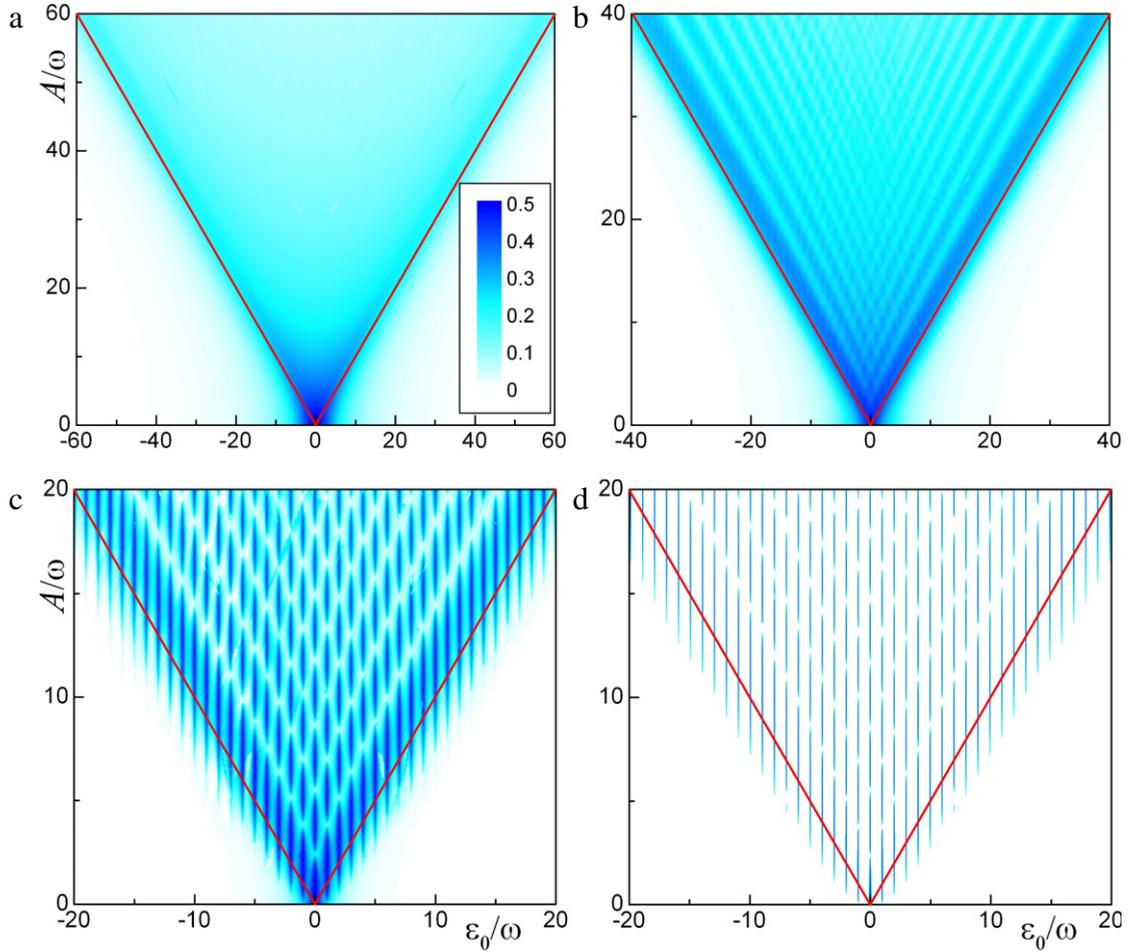
Fig. 10. (Color online) Same as in Fig. 7 (i.e. LZS interferometry with high-frequency driving), but including the effects of decoherence. The time-averaged upper diabatic state occupation probability $\overline{P}_{up}$ is obtained numerically by solving the Bloch equations with the Hamiltonian (1). The dephasing time T_2 is given by $\omega T_2/(2\pi) = 0.1$ in (a), 0.5 in (b), 1 in (c) and $T_2 = 2T_1$ in (d). The relaxation time is given by $\omega T_1/(2\pi) = 10^3$.

We now increase the coherence time further, such that interference between transitions from a few successive driving cycles occurs. We now start to see the resonance lines forming, or rather the mixing between the two states being suppressed whenever the resonance condition is not satisfied (Figs. 9(c) and 10(c)). Finally, in Figs. 9(d) and 10 (d) we take the case of negligible decoherence, and we find that the resonance lines are now well defined. Deviation from the resonance condition leads to the absence of any substantial mixing between the two states.

2.6. "Breakdown" of the adiabatic theorem

The adiabatic theorem is used in various subfields of physics. The basic idea of the theorem is the following (Landau and Lifshitz, 1977): if a physical system starts in one of the eigenstates of the system's Hamiltonian, the Hamiltonian is varied slowly enough and there are no degeneracies between the eigenstates during the variation of the Hamiltonian, then the system will end up in an eigenstate of the Hamiltonian whose order (starting from the ground state counting upwards) is the same as that of the initial state.

As the term "theorem" suggests, the above statement is a rigorously provable statement. The tricky point is in deciding how slow the Hamiltonian variation must be in order to ensure adiabaticity. The most common form of the adiabatic condition is obtained by inspecting the LZ formula (Eq. (19)): $\delta \gg 1$, and slightly generalized forms of this condition. If the condition $\delta \gg 1$ is satisfied in the LZ problem, the system will almost certainly stay in the ground state, assuming it started in the ground state. The problem is that the above condition was derived for a specific problem, namely the simple LZ problem, and not from general considerations that apply to any quantum system with any form of Hamiltonian variation. This issue has been the subject of a number of recent papers (Marzlin and Sanders, 2004; Sarandy et al., 2004; Tong et al., 2005, 2007; Amin, 2009). For example, if a many-level system starts in an eigenstate of the Hamiltonian, and then during the variation of the Hamiltonian an enormously large number of avoided level crossings are encountered (in what can colloquially be

called a "spaghetti" energy-level structure), as e.g. in Pokrovsky and Sinitsyn (2002, 2004), Shytov (2004) and Garanin et al. (2008), knowing that each crossing depletes the population of the initial eigenstate by a small amount does not guarantee that the total depletion of the state from all the crossings will also be small.

Another example where the above simple condition does not guarantee adiabaticity over the full time evolution occurs in the simple LZS interferometry setup considered in this review. If the system is repeatedly driven back and forth across the avoided-crossing point and the phase accumulated between successive crossings is designed to produce constructive interference, the small transition amplitudes of the different crossings will add up to produce a large transition probability. For example, if we take $\delta \gg 1$, $\varepsilon_0 = 0$ and $A/\omega = \pi/2 + k\pi$ (i.e., we choose the parameters to satisfy the resonance condition, Eq. (43)), we know that it is only a matter of time until the ground-state population is transferred completely to the excited state and vice versa. Finally, it should be emphasized that one does not need to satisfy any resonance condition of the kind given in Eq. (37). An arbitrary-looking driving signal that produces suitable phase accumulation between successive crossings will also eventually result in full population transfer between the ground and excited states. Even *random* phases will result in diffusion-like dynamics that ultimately result in large mixing between eigenstates.

When discussing the adiabatic theorem, it is worth digressing for a moment to mention an idea that has received considerable attention recently, namely adiabatic quantum computing (AQC) (Farhi et al., 2001). The basic idea of AQC is as follows: one subjects a physical system to a simple initial Hamiltonian, such that it is guaranteed that the system will relax to its ground state. One then adiabatically changes the Hamiltonian to reach a final Hamiltonian whose ground state encodes the answer a given problem (the specifics of the problem are encoded in the parameters of the final Hamiltonian). Measuring the final state then provides the answer to the problem. During the evolution from the initial to the final Hamiltonian, one can expect that avoided crossing structures will be encountered, and the size and number of these avoided crossings will determine the requirements on the sweep rate. The smaller the energy gaps and the larger the number of crossings, the more slowly one has to sweep the parameters of the Hamiltonian. The traversal of the avoided crossings is governed by LZ physics, and non-adiabatic LZ transitions play a destructive role and should be avoided; this was studied for a superconducting qubit e.g. in Grajcar et al. (2005). It is currently unknown how the running time scales with system size for different problems. The answer to this question will determine whether AQC provides a computational advantage over classical computers or not. In a study that comes a step closer to the subject of the present article, it was argued in Ashhab et al. (2006) that the interaction between an AQC system and its surrounding environment could lead to a situation where the environment effectively drives the system back and forth across the avoided crossings, thus reducing the probability of remaining in the ground state.

2.7. Reversal of stimulated emission

It is well known that when an atom is placed in a resonant cavity and the atom is initialized in its excited state, it emits a photon into the cavity with a rate that is proportional to the number of photons in the cavity (more accurately, the emission rate is proportional to $n + 1$, where n is the number of photons in the cavity). Recently, this situation was realized in an experiment that uses a superconducting charge qubit whose energy-level structure is essentially the one that we study here (Astafiev et al., 2007). The qubit is biased such that it experiences an effective inverted relaxation taking it from the ground to the excited state. The qubit therefore constantly emits photons into the resonant cavity, and a lasing state is realized.

As discussed in Ashhab et al. (2009), for small photon numbers the emission rate is proportional to the number of photons in the cavity, which can be seen as being a result of the fact that the Rabi frequency is proportional to the square-root of the photon number. It is interesting to consider what happens if the photon number is so large that the cavity field effectively drives the qubit back and forth across the quasi-crossing region. In this case the Rabi frequency is no longer proportional to the driving amplitude (which is proportional to the square-root of the photon number), but it follows the Bessel-function dependence that is characteristic of LZS interferometry (see Appendix C). One therefore has the situation where the emission rate is no longer proportional to the photon number in the cavity n, but rather it is proportional to $J_1^2(\alpha\sqrt{n})$, where α is a conversion coefficient. Stimulated emission therefore exhibits oscillatory behavior, where the emission rate has regions where it increases with increasing photon number and regions where it decreases with increasing photon number.

One consequence of the quasi-periodicity in the Bessel function is that, with a suitable choice of parameters, there can exist several stable steady-state photon numbers in the cavity. These solutions can be obtained by comparing the emission rate into the cavity (which follows the Bessel-function dependence) and the loss rate out of the cavity (which is proportional to the photon number). This situation concerning the existence of multiple steady-state solutions in this system was studied in Rodrigues et al. (2007a,b).

3. Recent experiments with strongly driven superconducting quantum circuits

3.1. Multiphoton transitions in superconducting qubits

If a quantum system is strongly driven, it can be excited by a multiphoton process. One way to observe the multiphoton resonances is to consider the frequency dependence, which is convenient for atoms exposed to a periodic electromagnetic field (Gallagher, 1994; Fregenal et al., 2004; Førre, 2004; Maeda et al., 2006). Another way is to tune the energy difference at

fixed driving frequency. In superconducting qubits the energy difference is tuned by an external source. The observation of the resonances allows for multiphoton spectroscopy. Furthermore, the strong driving provides a tool to control the energy level population, with the driving frequency being a fraction of the energy level difference. This is important for operating superconducting qubits, where the energy difference is of the order of 0.1 to 10 GHz. The multiphoton resonances have Lorentzian shapes (Tornes and Stroud, 2008), as described by Eqs. (55) or (57), which provide a way to estimate the relaxation rates in the system.

Multiphoton resonances were observed in several superconducting qubits with a small number of photons. They were observed in charge qubits (Nakamura et al., 2001), where the energy-level difference is controlled by a gate voltage, as well as in the charge-phase qubits, where the energy difference is controlled by both a gate voltage and an external magnetic flux (Shnyrkov et al., 2006, 2009). Up to five-photon transitions were reported for the phase qubit (Wallraff et al., 2003), where the energy difference is tuned by the bias current. Multiphoton transitions were also observed in a flux qubit (Saito et al., 2004) controlled by an external magnetic flux. Further improvement of the coherence characteristics of the superconducting qubits allowed to observe resonant excitations with more photons, at higher driving amplitudes. These results are presented below.

3.2. LZS interferometry in superconducting qubits

The observation of LZ tunneling in superconducting qubits was first reported by Izmalkov et al. (2004) and then by Ithier et al. (2005) and Johansson et al. (2009) (see also Ankerhold and Grabert (2003) for the theoretical background). Recently LZS interferometry was demonstrated by several groups on different superconducting qubits with complementary measurement techniques (Oliver et al., 2005; Sillanpää et al., 2006; Wilson et al., 2007; Izmalkov et al., 2008; LaHaye et al., 2009). Below we briefly describe these works and present the major results in Fig. 11. There, the left column shows the circuits used in the experimental setups and the right columns shows their corresponding experimental LZS interferometry. The latter shows a measurable quantity versus driving power (amplitude) and energy bias (which defines the energy level distance). Also recently the LZS interferometry was demonstrated with the rf SQUID qubit in Sun et al. (2009) [see also Sun et al. (2006) for experimental details]. One important difference from the previous works is that the system is essentially a multi-level system with several different avoided crossings involved (see also next subsection). This allows for additional interesting and useful phenomena such as controllable population inversion, as convincingly demonstrated both experimentally and theoretically in Sun et al. (2009).

The parameters used in different experiments studying LZS interferometry with driven superconducting qubits are given in Table 1. Remarkable is the fact that in all of these experiments the relation of the characteristic time of the LZ transition (Eq. (21)) estimated with maximal driving amplitude $A^{\max}$, $t_{\mathrm{LZ}} \sim 1/\sqrt{A^{\max}\omega}$, to the driving period T was almost identical: $t_{\mathrm{LZ}}/T \sim 0.05$. Note that the exact value of t_{LZ}/T does not affect the analysis or results, provided that this ratio is much smaller than one (see Eq. (30)).

(1) In Ref. Oliver et al. (2005) a superconducting flux qubit was subjected to a strong microwave drive and LZS multiple interference fringes were observed. The flux qubit was a niobium superconducting ring with three Josephson junctions. The circuit and results are shown in Fig. 11(a) to the left and to the right respectively. The qubit was biased with both dc and microwave magnetic fluxes. The level population was probed with a dc SQUID. The switching probability of the SQUID to the resistive state measures the state of the qubit in the diabatic basis $\{\varphi_\uparrow, \varphi_\downarrow\}$. These measurements showed resonant peaks and dips when the energy of k photons matched the qubit's energy-level difference. The latter was controlled with the dc flux (flux detuning) and multiphoton resonances with k up to 20 were observed. Later the observation of multiphoton resonances of order up to 45 was reported (Berns et al., 2006). The interference fringes shown in Fig. 11 are described by the theory presented in Section 2.4.2; cf. also Fig. 7(a). The fringes exhibit the Bessel-function dependence, according to Eqs. (52) and (55), and the steplike pattern in Fig. 11(a) was called a "Bessel staircase" (Oliver et al., 2005); the inclined white lines in Fig. 11(a) show the maxima for $J_k^2(A/\omega)$ which were numbered with the Roman numbers I to VI. For more details see Rudner et al. (2008), Bylander et al. (2009) and Oliver and Valenzuela (2009).

(2) In Ref. Sillanpää et al. (2006) an interferometer-type charge qubit was studied. The qubit consisted of two nearby Josephson junctions embedded in a loop (Fig. 11(b)). The charge on the island between the junctions (the so-called Cooper-pair box) was controlled via the applied gate voltage $V_g = en_g/C_g$, $n_g(t) = n_{g0} + \delta n_{\mathrm{rf}} \sin(\omega_{\mathrm{rf}} t)$. The effective Josephson energy of the two junctions was tuned using the applied magnetic flux Φ through the loop. The energy levels of the qubit were controlled by the flux Φ and by the dc component (n_{g0}) of the voltage, while the energy-level populations were controlled by the ac component of the voltage. The qubit was coupled in parallel to an LC-circuit. The effective capacitance C_{eff} of the qubit modifies the resonant frequency of the LC-circuit (Sillanpää et al., 2005). This provides a method for the continuous-time monitoring of the qubit's effective capacitance, which is related to the occupations of the qubit's energy eigenstates. The resulting LZS interference pattern is shown to the right in Fig. 11(b); this is described by the theory presented in Section 2.4.1; cf. also Fig. 6. For more details see also Paila et al. (2009) and Sillanpää et al. (2007). Also very recently LZS interferometry with an interferometer-type charge qubit was demonstrated in LaHaye et al. (2009). The parameters of the qubit were close to the ones in Ref. Sillanpää et al. (2006); consequently, LZS interference fringes were similar to the ones shown in Fig. 11(b). The important difference is in the measuring device: the qubit was coupled to a nanoelectromechanical resonator, as studied theoretically in Irish and Schwab (2003), and the nanoresonator frequency shift was measured.
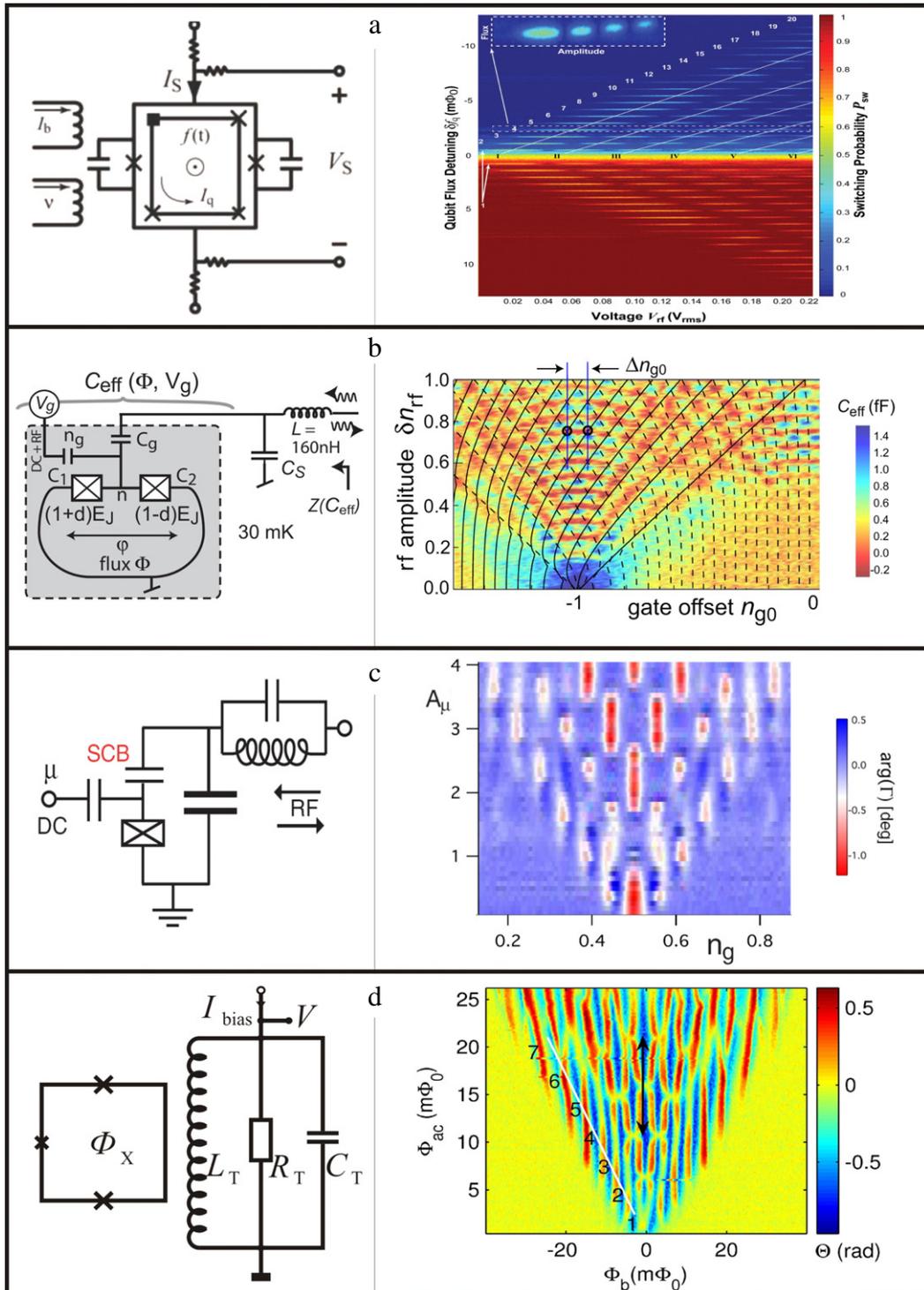
Fig. 11. (Color online) Experimentally realized Landau–Zener–Stückelberg (LZS) interferometry. The panels from top to bottom present the results of the following articles: (a) Oliver et al. (2005), (b) Sillanpää et al. (2006), (c) Wilson et al. (2007), (d) Izmalkov et al. (2008). Schematic diagrams of the circuits used are shown to the left, while results for the LZS interferometry are presented to the right. A more detailed description of the experiments can be found in the main text and, of course, in the respective original articles. Figure (a) is reprinted from Oliver et al. (2005) with permission from AAAS. Figure (b) is reprinted from Sillanpää et al. (2006) with permission; copyright (2006) by APS. Figure (c) is reprinted from Wilson et al. (2007) with permission; copyright (2007) by APS. Figure (d) is reprinted from Izmalkov et al. (2008) with permission; copyright (2008) by APS.

(3) References (Wilson et al., 2007, 2010) studied a single Cooper-pair box (SCB), which was composed of an aluminium island connected to a reservoir via a Josephson junction (Fig. 11(c)). The state of the qubit was controlled by the gate voltage V_g ($n_g = C_g V_g/2e$) and by the magnetic field in the dc SQUID loop connected to the island, which tunes the Josephson energy E_J. The qubit was driven through the gate with the microwave amplitude A_μ. The qubit state was probed with an rf oscillator (Duty et al., 2005; Persson et al., 2010). The color image in Fig. 11(c) presents the phase of the rf reflection coefficient Γ. The ground and excited states contributed phase shifts with opposite signs. The results were interpreted in terms of the dressed states of the qubit coupled to the driving microwave field (Liu et al., 2006; Greenberg, 2007).

(4) In Ref. Izmalkov et al. (2008) a superconducting flux qubit was driven by an external magnetic flux, analogously to Ref. Oliver et al. (2005). The qubit was weakly coupled to a classical resonant tank circuit, Fig. 11(d). The tank circuit was biased with an rf current I_{bias} and the measurable quantity was the phase shift Θ between the voltage V and the bias current in the tank circuit. The inductive coupling of the qubit to the tank circuit resulted in a phase shift determined by the effective inductance of the qubit (Greenberg et al., 2002; Il'ichev et al., 2009). The resonant excitation of the flux qubit changes the direction of the current in the qubit's loop, which resonantly changes the effective inductance of the qubit. The respective resonances were observed in the phase shift dependence as a sequence of the ridges and troughs (Shevchenko et al., 2008). The LZS interference pattern is shown in Fig. 11(d) in the dependence of the tank phase shift Θ on the dc (Φ_b) and ac (Φ_{ac}) components of the magnetic flux; the interference fringes are described by the theory presented in Section 2: see Fig. 7(b).

Thus, strongly driven superconducting qubits were studied by different, complementary methods; their resonant characteristics were shown to be periodic in the bias ε_0 and driving amplitude A due to Stückelberg oscillations. The different experimental measurements allowed to obtain the following parameters: (i) those which characterize the qubit and enter in the pseudo-spin Hamiltonian, (ii) the driving microwave amplitude as felt by the qubit (which is the calibration of a generator signal), (iii) the relaxation and dephasing rates, which describe the impact of the environment on the qubit dynamics (via the Bloch equations).

3.3. Multiphoton resonances in multi-level systems

Most qubits are formed by the lowest two levels in a multi-level structure. Moreover, a qubit can be coupled to another quantum system, in particular, to another qubit, so that the overall structure is also multi-level. High-amplitude driving allows not only to reach the upper level of a TLS (qubit) with the absorption of several photons, but also to involve more of the *qudit*'s energy levels in the process.

Multiphoton resonant excitations were studied in superconducting multi-level systems. One-, two-, and three-photon transitions were driven in the flux qubit not only between the two lowest levels (which form the qubit), but rather between five levels in Yu et al. (2005). In this case multiphoton spectroscopy allowed to obtain the system parameters and to visualize the energy-level diagram. The low-frequency and extremely strong-driving regime was studied in Berns et al. (2008) [see also Wilhelm (2008) and Wen and Yu (2009)]. Berns et al. demonstrated that their method, which they called amplitude spectroscopy, allows probing higher levels that are three orders of magnitude higher in energy than the driving frequency. Recently interference fringes associated with LZ transitions at two nearby avoided crossings were also observed in a multi-level structure of the rf-SQUID qubit driven by large-amplitude and high-frequency microwave field (Wang et al., 2010) [see also Sun et al. (2009) for more details]. Also, multiphoton multi-level Rabi oscillations were studied in a phase qubit (Dutta et al., 2008). Multiphoton transitions in the multilevel system formed by the dressed states of a qubit coupled to a quantum resonator were demonstrated in Fink et al. (2009) and Bishop et al. (2009). Another situation where a multi-level structure appears, is a system of coupled qubits. Direct and ladder-type multiphoton excitations were recently demonstrated in a two-flux-qubit system in Il'ichev et al. (2010).

4. Conclusions

Strong driving of a TLS results in a periodic dependence of its response on the bias, driving frequency and amplitude. This dependence was recently observed in superconducting qubit systems by several groups using complementary measurement techniques, both in flux qubits (Oliver et al., 2005; Izmalkov et al., 2008) and in charge qubits (Sillanpää et al., 2006; Wilson et al., 2007). Very recently LZS interferometry was also realized in a rf SQUID qubit (Sun et al., 2009). No related effect has been reported in experiments using phase qubits. This is because it is difficult to produce avoided energy-level structures in phase qubits without involving higher levels.

LZS interferometry allows, first, to control the qubit state, and, second, to obtain the system parameters. In particular, from the positions of the multiphoton resonances, the qubit parameters can be obtained (spectroscopy); the Stückelberg oscillations can be used for the definition of the driving amplitude (calibration of power); and the width and shape of the interference fringes can be used to estimate the relaxation rates. These properties make LZS interferometry a very powerful tool for studying TLSs (see also LaHaye et al. (2009), where LZS interferometry was realized recently for a superconducting qubit coupled to a nanoelectromechanical resonator).

We have reviewed recent experimental results on LZS interferometry, and we have presented the theoretical description of this problem. In particular, we have demonstrated the applicability of the adiabatic-impulse model for both slow and fast driving regimes. This model is a powerful tool in the study of non-adiabatic transitions at avoided crossings and the interference between these transitions.

Acknowledgements

Appendix A. Solution of the Landau–Zener problem

A.1. Adiabatic wave function

In this Appendix we consider the driven two-level system in the adiabatic representation, assuming the evolution to be adiabatic far from the avoided level crossings, with non-adiabatic transitions occurring around these points.

The wave function in the adiabatic approximation takes the form

$$\psi = \begin{pmatrix} a_1 \\ a_2 \end{pmatrix}, \quad a_{1,2} = A_{1,2} \exp\left(-i \int E(t) dt\right). \tag{A.1}$$

Then the Shrödinger equation $H\psi = E\psi$ gives the instantaneous eigenvalues, Eq. (4), and eigenvectors:

$$\psi_\pm = \varphi_\pm e^{\mp i(\zeta + \frac{\pi}{4})}, \qquad \zeta = \frac{1}{2} \int \Omega(t) dt, \tag{A.2a}$$

$$\varphi_\pm = \begin{pmatrix} \beta_\mp \\ \mp\beta_\pm \end{pmatrix}, \qquad \beta_\pm = \sqrt{\frac{\Omega \pm \varepsilon}{2\Omega}}. \tag{A.2b}$$

Here the term $\pi/4$ arises when the next term in the quasiclassical (adiabatic) approximation is taken into account (Delone and Krainov, 1985).

Let us consider the original LZ problem described by the Hamiltonian (1) with $\varepsilon = vt$ {see also Eq. (17); we consider t instead of t' in this Appendix}:

$$H(t) = -\frac{\Delta}{2}\sigma_x - \frac{vt}{2}\sigma_z. \tag{A.3}$$

Consider now the adiabatic wave function in the region far from the avoided level crossing, where $|\varepsilon(t)| = v|t| \gg \Delta$. Note that this latter condition is consistent with the condition $\omega|t| \ll 1$ used for the linearization of the harmonic-driving problem, Eq. (15), at large enough driving amplitudes. Then we have:

$$\varphi_+ \approx \begin{pmatrix} 1 \\ 0 \end{pmatrix}, \qquad \varphi_- \approx \begin{pmatrix} 0 \\ 1 \end{pmatrix} \quad \text{if } t_a < 0, \tag{A.4a}$$

$$\varphi_+ \approx \begin{pmatrix} 0 \\ -1 \end{pmatrix}, \qquad \varphi_- \approx \begin{pmatrix} 1 \\ 0 \end{pmatrix} \quad \text{if } t_a > 0, \tag{A.4b}$$

$$\zeta(\pm t_a) = \frac{1}{2} \int_0^{\pm t_a} \Omega(t) \, dt \approx \pm\left[\Phi\left(\sqrt{\frac{v}{2}} t_a\right) - \Phi_\delta\right]. \tag{A.5}$$

The subscript "a" indicates that we now consider the time within the asymptotic region, where $|\varepsilon(t)| \gg \Delta$, and the acquired phase was split into time-dependent and independent parts:

$$\Phi(z_a) = \frac{z_a^2}{2} + \delta \ln(\sqrt{2}z_a), \tag{A.6}$$

$$\Phi_\delta = \frac{1}{2}\delta(\ln\delta - 1). \tag{A.7}$$

A.2. Non-adiabatic transition (evolution matrix for the Landau–Zener transition)

Let us now consider the non-adiabatic transition between the energy levels in the vicinity of the point of avoided level crossings, following Zener (1932). Then the Schrödinger equation $i\dot{\psi} = H\psi$ takes the form:

$$\begin{cases} i\dot{a}_1 = -\dfrac{v}{2}ta_1 - \dfrac{\Delta}{2}a_2, \\ i\dot{a}_2 = -\dfrac{\Delta}{2}a_1 + \dfrac{v}{2}ta_2. \end{cases} \tag{A.8}$$

This can be written in the form of the second-order Weber equations:

$$\frac{d^2a_{1,2}}{dz^2} + (2\delta \mp i + z^2)a_{1,2} = 0, \tag{A.9}$$

$$z = \sqrt{\frac{v}{2}}t. \tag{A.10}$$

The solutions are combinations of parabolic cylinder functions (Gradshteyn and Ryzhik, 1994):

$$a_1 = \sum_{\pm} A_{\pm} D_{-1-i\delta}(\pm\sqrt{2}e^{i\pi/4}z), \tag{A.11a}$$

$$a_2 = \sum_{\pm} B_{\pm} D_{-i\delta}(\pm\sqrt{2}e^{i\pi/4}z). \tag{A.11b}$$

We find the relation between the coefficients $A_{\pm}$ and $B_{\pm}$ from the first-order equation (by inserting the solutions for $a_{1,2}$ in the first equation of the system (A.8)) making use of the recurrence formula:

$$B_{\pm} = \mp\frac{e^{-i\pi/4}}{\sqrt{\delta}}A_{\pm}. \tag{A.12}$$

Now with the asymptotes of the parabolic cylinder functions (Gradshteyn and Ryzhik, 1994), we find $a_{1,2}$ far from the transition point (where $z = 0$), at $z = \pm z_a$ with $z_a \gg 1$:

$$a_1(-z_a) \approx A_+ \Xi_1 e^{i\Phi(z_a)}, \tag{A.13a}$$

$$a_2(-z_a) \approx (-e^{-\frac{\pi}{2}\delta}A_+ + e^{\frac{\pi}{2}\delta}A_-)\Xi_2 e^{-i\Phi(z_a)}, \tag{A.13b}$$

$$a_1(z_a) \approx A_- \Xi_1 e^{i\Phi(z_a)}, \tag{A.13c}$$

$$a_2(z_a) \approx (-e^{\frac{\pi}{2}\delta}A_+ + e^{-\frac{\pi}{2}\delta}A_-)\Xi_2 e^{-i\Phi(z_a)}, \tag{A.13d}$$

where

$$\Xi_1 \equiv \frac{\sqrt{2\pi}}{\Gamma(1+i\delta)} \exp\left(-\frac{\pi}{4}\delta\right), \tag{A.14a}$$

$$\Xi_2 \equiv \frac{1}{\sqrt{\delta}} \exp\left(-i\frac{\pi}{4} - \frac{\pi}{4}\delta\right). \tag{A.14b}$$

Let us match this asymptotic solution with the adiabatic one, $\psi(t) = \sum b_{\pm}\varphi_{\pm}$, from the previous subsection:

$$\begin{pmatrix} b_+ \\ b_- \end{pmatrix} = \begin{pmatrix} a_1 \\ a_2 \end{pmatrix} \quad \text{at } t_a < 0, \tag{A.15a}$$

$$\begin{pmatrix} b_- \\ -b_+ \end{pmatrix} = \begin{pmatrix} a_1 \\ a_2 \end{pmatrix} \quad \text{at } t_a > 0. \tag{A.15b}$$

Here the time dependence in the l.h.s. and in the r.h.s. is the same, see respectively Eqs. (A.5) and (A.13). This allows to describe the evolution from $t = -t_a$ to t_a as a sequence of adiabatic evolutions from $t = -t_a$ to $t = -0$ and from $t = +0$ to $t = t_a$, with the nonadiabatic transition in between (described by the time-independent matrix N), namely:

$$\mathbf{b}(t_a) = U(t_a, +0)NU(-0, -t_a)\,\mathbf{b}(-t_a) = e^{-i\sigma_z\zeta(t_a)}Ne^{-i\sigma_z\zeta(t_a)}\mathbf{b}(-t_a). \tag{A.16}$$

Then collecting this with Eqs. (A.15) and (A.13) and equating multipliers with A_+ and A_-, we obtain the expression (24) for the matrix N. This matrix describes the transition between the two adiabatic states with the probability given by Eq. (19) and also includes the phase jump $\widetilde{\varphi}_S$. We note that the matrix N at $t = t_2$ is the same as at $t = t_1$ for the nonadiabatic transitions.

The argument of the asymptotes of the gamma function Γ are (Gradshteyn and Ryzhik, 1994):

$$\arg \Gamma(1-i\delta) \approx \begin{cases} C\delta, & \delta \ll 1, \\ -\dfrac{\pi}{4} - \delta(\ln\delta - 1), & \delta \gg 1, \end{cases} \tag{A.17}$$

where $C \approx 0.58$ is the Euler constant. Thus, the phase jump $\varphi_S(\delta)$ is a monotonous function, which changes from 0 in the adiabatic limit ($\delta \gg 1$) to $\pi/4$ in the diabatic (fast driving) limit ($\delta \ll 1$).

It is worth making a comment on bases here. In this review we have used the energy eigenbasis for describing the dynamics of the TLS. Furthermore, we have followed the reasonable convention where the ground state far to the right of the avoided crossing region coincides with the excited state far to the left of the avoided crossing region, and vice versa. In principle, we could have defined these pairs of states such that they differ by some phase factors. If we follow such a convention, there would be some asymmetry between the different matrices (denoted by N) that describe the different LZ transitions. However, since such a convention seems rather unnatural, we do not comment on it further. A different convention from ours that appears more frequently in the literature is the use of the diabatic states for describing the dynamics. In this case the matrices that describe the evolution from time $-t_a$ to time t_a for a single passage depend on the signs that appear in the Hamiltonian, Eq. (17). The part describing the dynamical phase accumulated during the adiabatic parts of the evolution is straightforward. The LZ transition matrices are less obvious, and we give the rules for how to determine them explicitly here. For the Hamiltonian in Eq. (17) with negative signs in front of both terms in the Hamiltonian, the LZ transition matrix takes the form:

$$\begin{pmatrix} \sqrt{P_{LZ}} & \sqrt{1-P_{LZ}}e^{i\varphi_S} \\ -\sqrt{1-P_{LZ}}e^{-i\varphi_S} & \sqrt{P_{LZ}} \end{pmatrix}. \tag{A.18}$$

If the sign in front of the second term in the Hamiltonian is reversed, the off-diagonal matrix elements in Eq. (A.18) are reversed. If the sign in front of the first term in the Hamiltonian is reversed, only the minus sign at the beginning of the bottom-left matrix element is moved to the top-right matrix element. Combining the two rules above, if both signs in the Hamiltonian are reversed, only the minus sign in front of the Stokes phase is moved from the bottom-left matrix element to the top-right matrix element. Note that in the diabatic basis there will always be two relevant signs in front of the second term in the Hamiltonian, depending on whether the avoided crossing is traversed from left to right or from right to left. As a result, there will be two different matrices describing the different crossings.

Appendix B. Evolution of a periodically driven two-level system

The time evolution of a periodically driven TLS is described by Eqs. (31) and (32). Consider first the matrix for a one-period evolution:

$$NU_2NU_1 = \begin{pmatrix} \alpha & -\gamma^* \\ \gamma & \alpha^* \end{pmatrix}, \tag{B.1a}$$

$$\alpha = (1 - P_{LZ})e^{-i\zeta_+} - P_{LZ}e^{-i\zeta_-}, \tag{B.2a}$$

$$\gamma = \sqrt{P_{LZ}(1 - P_{LZ})}e^{i\widetilde{\varphi}_S}(e^{-i\zeta_+} + e^{-i\zeta_-}), \tag{B.2b}$$

$$\zeta_+ = \zeta_1 + \zeta_2 + 2\widetilde{\varphi}_S, \tag{B.3a}$$

$$\zeta_- = \zeta_1 - \zeta_2. \tag{B.3b}$$

After diagonalizing the matrix, it is straightforward to write down its nth power, e.g. Bychkov and Dykhne (1970). This unitary evolution matrix $(NU_2NU_1)^n$ has the form

$$(NU_2NU_1)^n = \begin{pmatrix} u_{11} & -u_{21}^* \\ u_{21} & u_{11}^* \end{pmatrix}, \tag{B.3c}$$

with elements:

$$u_{11} = \cos n\phi + i(\text{Im}\,\alpha)\frac{\sin n\phi}{\sin \phi}, \tag{B.4a}$$

$$u_{21} = \gamma \frac{\sin n\phi}{\sin \phi}, \tag{B.4b}$$

$$\cos \phi = \text{Re}\,\alpha. \tag{B.4c}$$

Then with Eq. (31) for $(t - 2\pi n/\omega) \in (t_1, t_2)$, we obtain the upper-level occupation probability, $P_+ = |b_+|^2$,

$$P_+^{(I)}(n) = |\gamma|^2 \frac{\sin^2 n\phi}{\sin^2 \phi}. \tag{B.5}$$

And for $(t - 2\pi n/\omega) \in (t_2, t_1 + 2\pi/\omega)$ with Eq. (32) we obtain:

$$P_+^{(II)}(n) = 2Q_1 \frac{\sin^2 n\phi}{\sin^2 \phi} + Q_2 \frac{\sin 2n\phi}{\sin \phi} + P_{LZ} \cos 2n\phi, \tag{B.6}$$

$$Q_1 = P_{LZ} \left[P_{LZ} \sin^2 \zeta_- + (1 - P_{LZ})(1 + \cos \zeta_+ \cos \zeta_-) \right], \tag{B.7a}$$

$$Q_2 = 2 P_{LZ}(1 - P_{LZ}) \cos(\zeta_1 + \widetilde{\varphi}_S) \cos(\zeta_2 + \widetilde{\varphi}_S). \tag{B.8}$$

Now the time-averaging corresponds to averaging over $n \gg 1$ periods and, from Eqs. (B.5) and (B.6), we obtain:

$$\overline{P_+^{(I)}} = \frac{|\gamma|^2}{2 \sin^2 \phi} = \frac{1}{2} \frac{|\gamma|^2}{|\gamma|^2 + (\mathrm{Im}\alpha)^2}, \tag{B.9}$$

$$\overline{P_+^{(II)}} = \frac{Q_1}{\sin^2 \phi}. \tag{B.10}$$

From Eq. (B.9) it follows that the upper-level occupation probability is maximal at $\mathrm{Im}\alpha = 0$. This results in the general resonance condition:

$$(1 - P_{LZ}) \sin \zeta_+ - P_{LZ} \sin \zeta_- = 0. \tag{B.11}$$

In particular, in the slow and fast limits the resonance condition takes the form:

$$\zeta_1 + \zeta_2 = k\pi \quad \text{for } 2\pi\delta \gg 1, \tag{B.12a}$$

$$\zeta_1 - \zeta_2 = k\pi \quad \text{for } 2\pi\delta \ll 1. \tag{B.12b}$$

The resonance condition (B.11) was derived in Ashhab et al. (2007) using an alternative, geometric visualization of the dynamics. There, the evolution matrix for one full driving period, i.e. $(NU_2 NU_1)$, is decomposed into two rotations, a rotation around an axis in the xy plane followed by a rotation around the z-axis. The resonance condition is then identified as the requirement that the z-axis rotation does not affect the dynamics, i.e. the z-axis rotation is a rotation by a multiple of 2π. Straightforward algebra then gives Eq. (B.11). A related alternative derivation of the resonance condition relies on visualizing the evolution matrix for one full driving period as a single rotation: on resonance the rotation axis lies in the xy-plane.

First, let us consider the case of the *slow-passage limit*, where $\delta \gg 1$ and $P_{LZ} \ll 1$. We now neglect the difference between $\overline{P_+^{(I)}}$ and $\overline{P_+^{(II)}}$ and, from Eq. (B.10) to the lowest order approximation in P_{LZ}, we obtain:

$$\overline{P_+} = \frac{P_{LZ}(1 + \cos \zeta_+ \cos \zeta_-)}{\sin^2 \zeta_+ + 2 P_{LZ}(1 + \cos \zeta_+ \cos \zeta_-)}. \tag{B.13}$$

For small offset $\varepsilon_0 / A \ll 1$ the expressions for $\zeta_\pm$ can be simplified: $\zeta_1 + \zeta_2 \approx 2A/\omega$, $\zeta_1 - \zeta_2 \approx \pi \varepsilon_0 / \omega$. This makes Eq. (B.13) analogous to the result obtained in Shytov et al. (2003) (their Eq. (20) at $u = w \to 0$). But for arbitrary (not small) offset ε_0 one has to make use of Eq. (B.13) with $\zeta_\pm$ given by Eqs. (B.3) and (14); the result, such as Fig. 6 is significantly dependent on this correction.

One can also obtain an idea about the form of the resonance condition in the zeroth in Δ/ε_0 approximation:

$$\begin{aligned} \zeta_1 &\approx \frac{1}{2} \int_{t_1}^{t_2} \varepsilon(t) \mathrm{d}t \\ &= \frac{\pi \varepsilon_0}{\omega} - \frac{\varepsilon_0}{\omega} \cos^{-1} \frac{\varepsilon_0}{A} + \frac{\sqrt{A^2 - \varepsilon_0^2}}{\omega}, \end{aligned} \tag{B.14a}$$

$$\zeta_2 \approx -\frac{\varepsilon_0}{\omega} \cos^{-1} \frac{\varepsilon_0}{A} + \frac{\sqrt{A^2 - \varepsilon_0^2}}{\omega}. \tag{B.14b}$$

Eq. (B.12a) then gives

$$\frac{\varepsilon_0}{\omega} + 2 \frac{\sqrt{A^2 - \varepsilon_0^2}}{\pi \omega} - 2 \frac{\varepsilon_0}{\pi \omega} \cos^{-1} \frac{\varepsilon_0}{A} = k. \tag{B.15}$$

We emphasize, however, that the above equation should be seen as a limiting case for small Δ that demonstrates the complicated form of the resonance condition.

Now consider the case of *fast passage*, where $(1 - P_{LZ}) \approx 2\pi\delta \ll 1$. The fast limit ($\delta \ll 1$) assumes a small value of Δ. In this limit there is a large probability ($P_{LZ} \sim 1$) for transitions between the adiabatic states in a single-passage; while the transition probability between diabatic states is small, $(1 - P_{LZ}) \ll 1$. Hence, we will consider the time-averaged probability of the upper diabatic state P_{up}. Note that upper diabatic state is $\varphi_\uparrow$ for $\varepsilon_0 < 0$ and $\varphi_\downarrow$ for $\varepsilon_0 > 0$. Let us consider the latter case, as shown in Fig. 1. Then we can relate P_{up} to $P_+^{(I)}$ and $P_+^{(II)}$ as follows:

$$P_{\mathrm{up}} \approx P_+^{(I)} \quad \text{for } (t - 2\pi n/\omega) \in (t_1, t_2), \tag{B.16}$$

$$P_{\mathrm{up}} \approx 1 - P_+^{(II)} \quad \text{for } (t - 2\pi n/\omega) \in (t_2, t_1 + 2\pi/\omega). \tag{B.17}$$

Then we note that $1 - P_+^{(II)} \approx P_+^{(I)}$ and obtain:

$$\overline{P}_{\text{up}} = \frac{1}{2} \frac{4\cos^2(\zeta_2 - \pi/4)}{\sin^2 \zeta_- + 4\cos^2(\zeta_2 - \pi/4)}, \tag{B.18}$$

where ζ_2 is given by Eq. (B.14b). On resonance $\zeta_- = k\pi$ and $\overline{P}_{\text{up}} = 1/2$, then with $\zeta_- \approx \pi \varepsilon_0/\omega$ for small offset ($\varepsilon_0/A \ll 1$) we obtain the resonance frequency $\omega^{(k)} = \varepsilon_0/k$. Consider now the vicinity of the kth resonance, introducing a small frequency detuning as follows

$$\delta\omega = k\omega - \varepsilon_0. \tag{B.19}$$

Then to first approximation in ε_0/A, we obtain:

$$\overline{P}_{\text{up}}^{(k)} = \frac{1}{2} \frac{\Delta_k^2}{\Delta_k^2 + \delta\omega^2}, \tag{B.20a}$$

$$\Delta_k = \Delta \sqrt{\frac{2\omega}{\pi A}} \cos\left(\frac{A}{\omega} - \frac{\pi}{4}(2k+1)\right). \tag{B.20b}$$

The total probability $\overline{P}_{\text{up}}$ is obtained as the sum of the partial contributions $\overline{P}_{\text{up}}^{(k)}$. This result, obtained in the adiabatic-impulse model, coincides with the one obtained within the RWA, Eqs. (55) and (56).

Appendix C. Rotating-wave approximation

C.1. Hamiltonian in the RWA-form

Following Pegg and Series (1973), Lopez-Castillo et al. (1992), Oliver et al. (2005) and Ashhab et al. (2007) we consider the rotating-wave approximation (RWA).

First, we split the Hamiltonian into time-independent and time-dependent parts:

$$H = -\frac{\Delta}{2}\sigma_x - \frac{\varepsilon_0 + A\cos\omega t}{2}\sigma_z = H_0 + V(t), \tag{C.1}$$

$$H_0 = -\frac{\Delta}{2}\sigma_x - \frac{\varepsilon_0}{2}\sigma_z, \tag{C.2a}$$

$$V(t) = -\frac{A\cos\omega t}{2}\sigma_z. \tag{C.2b}$$

Here we consider the time-dependent term with a cosine function (in contrast to the sine function used in Eq. (2)) because this choice agrees with the standard convention in the literature. The difference between the two choices is simply a shift of ωt by $\pi/2$, and it does not change the time-averaged probabilities which are of most interest to us.

Then we make a transformation to a rotating frame with the operator W:

$$W(t) = \exp\left(-\mathrm{i}\int V(t)\mathrm{d}t\right) = \exp\left(\mathrm{i}\frac{\eta(t)}{2}\sigma_z\right), \tag{C.3}$$

$$\eta(t) = \frac{A}{\omega}\sin\omega t. \tag{C.4}$$

This operator matches the wave function in the reference frame ψ with the wave function in the rotating frame ψ': $\psi = W(t)\psi'$. Then the Shrödinger equation in the rotating frame reads: $\mathrm{i}\dot{\psi}' = H'\psi'$ with

$$H' = W^\dagger H_0 W = -\frac{\Delta}{2}(\mathrm{e}^{-\mathrm{i}\eta(t)}\sigma_+ + h.c.) - \frac{\varepsilon_0}{2}\sigma_z, \tag{C.5}$$

$\sigma_+ = \sigma_x + \mathrm{i}\sigma_y$. Making use of the formula

$$\mathrm{e}^{\mathrm{i}x\sin\tau} = \sum_{n=-\infty}^{\infty} J_n(x)\,\mathrm{e}^{\mathrm{i}n\tau}, \tag{C.6}$$

the new Hamiltonian takes the form

$$H' = -\sum_{n=-\infty}^{\infty} \frac{\Delta_n}{2}\left(\mathrm{e}^{-\mathrm{i}n\omega t}\sigma_+ + h.c.\right) - \frac{\varepsilon_0}{2}\sigma_z, \tag{C.7}$$

$$\Delta_n = \Delta J_n(A/\omega). \tag{C.8}$$

Note that the unitary transformation W does not change the level occupation probabilities (the absolute values of the spinor components):

$$\psi = \begin{pmatrix} \psi_1 \\ \psi_2 \end{pmatrix} = W\psi' = e^{i\frac{\eta}{2}\sigma_z} \begin{pmatrix} \psi_1' \\ \psi_2' \end{pmatrix} = \begin{pmatrix} e^{i\frac{\eta}{2}}\psi_1' \\ e^{-i\frac{\eta}{2}}\psi_2' \end{pmatrix}. \tag{C.9}$$

C.2. Solving the Schrödinger equation in the absence of relaxation

Let us now study first the system without relaxation. We now look for a solution of the Schrödinger equation $i\dot{\psi}' = H'\psi'$ in the form:

$$\psi' = \begin{pmatrix} \psi_1'' \exp\left(-i\frac{k\omega t}{2}\right) \\ \psi_2'' \exp\left(i\frac{k\omega t}{2}\right) \end{pmatrix}. \tag{C.10}$$

Actually, this corresponds to the transformation: $\psi'' = \widetilde{W}(t)\psi'$ with $\widetilde{W}(t) = \exp(i\frac{k\omega t}{2}\sigma_z)$.

Consider now parameters close to the k-photon resonance, where $k\omega \approx \Delta E = |\varepsilon_0|$. In other words, we now consider the frequency detuning $\delta\omega = k\omega - \varepsilon_0$ to be small. The RWA consists in the assumption that, in the vicinity of the kth resonance, fast oscillating terms with $n \neq k$ can be neglected. Then the Schrödinger equation can be readily solved. The probability of the upper diabatic state (if the system was initially in the lower diabatic state) is given by:

$$\overline{P}_{\text{up}}^{(k)}(t) = |\psi_2(t)|^2 = \frac{1}{2}\frac{\Delta_k^2}{\delta\omega^2 + \Delta_k^2}\left(1 - \cos\sqrt{\delta\omega^2 + \Delta_k^2}\,t\right). \tag{C.11}$$

C.3. Solving the Bloch equations with relaxation

Now let us take into account relaxation by using the Bloch equations, which include two phenomenological relaxation times, T_1 and T_2 (Abragam, 1961). A convenient parametrization for the density matrix is the following:

$$\rho = \frac{1}{2}\begin{pmatrix} 1 + Z & X - iY \\ X + iY & 1 - Z \end{pmatrix}. \tag{C.12}$$

Here we note that the Bloch equations have to be written in the adiabatic (energy) representation, so that the constants T_1 and T_2 describe relaxation to the equilibrium values: $Z \to Z_0$ and $\rho_{21} = X + iY \to 0$. This representation differs from the diabatic representation (with the states $\{\varphi_\uparrow, \varphi_\downarrow\}$) by a small rotation with the angle $\Delta/\varepsilon_0 \ll 1$. Here we ignore this difference in the bases and consider the diabatic representation. Then for Z and $\rho_{21} = X + iY$, the Bloch equations with the Hamiltonian H' read:

$$\dot{Z} = -\Delta_k \text{Im}\left(e^{-ik\omega t}\rho_{21}\right) - \frac{Z - Z_0}{T_1}, \tag{C.13a}$$

$$\dot{\rho}_{21} = i\Delta_k e^{ik\omega t}Z - i\varepsilon_0\rho_{21} - \frac{\rho_{21}}{T_2}. \tag{C.13b}$$

(Again, we have neglected fast oscillating terms with $n \neq k$.) Here $Z_0 = \tanh\frac{\Delta E}{2T}$ describes the equilibrium energy level distribution at temperature T. After the substitution $\widetilde{\rho}_{21} = \rho_{21}\exp(ik\omega t) = \widetilde{X} + i\widetilde{Y}$, we obtain the system of equations:

$$\dot{\widetilde{X}} = \delta\omega\widetilde{Y} - \frac{\widetilde{X}}{T_2}, \tag{C.14a}$$

$$\dot{\widetilde{Y}} = -\delta\omega\widetilde{X} + \Delta_k Z - \frac{\widetilde{Y}}{T_2}, \tag{C.14b}$$

$$\dot{Z} = -\Delta_k\widetilde{Y} - \frac{Z - Z_0}{T_1}. \tag{C.14c}$$

The stationary solution of these equations is obtained after substituting $\dot{\widetilde{X}} = \dot{\widetilde{Y}} = \dot{Z} = 0$. Then the stationary value for the probability of the upper diabatic state is given by

$$\overline{P}_{\text{up}}^{(k)} = \overline{\rho}_{22} = \frac{1}{2}(1 - \overline{Z}), \tag{C.15}$$

$$\overline{Z} = \frac{1}{2}\frac{1 + T_2^2\delta\omega^2}{1 + T_2^2\delta\omega^2 + T_1 T_2\Delta_k^2}Z_0. \tag{C.16}$$

At low temperatures we can substitute $Z_0 \approx 1$ and obtain from Eqs. (C.15) and (C.16) the following formula

$$\overline{P}_{\mathrm{up}} = \sum_k \overline{P}_{\mathrm{up}}^{(k)} = \frac{1}{2} \sum_k \frac{\Delta_k^2}{\frac{1}{T_1 T_2} + \frac{T_2}{T_1} \delta\omega^2 + \Delta_k^2}, \tag{C.17}$$

which is useful for the description of multiphoton resonances at $\Delta/\varepsilon_0 \ll 1$.

Appendix D. Floquet theory

Floquet theory can be applied to any quantum system governed by a time-periodic Hamiltonian. The main idea of applying this theoretical approach is as follows: the time-dependent problem is turned into a time-independent one at the expense of increasing the effective number of states in the Hilbert space to an infinite number of states. Approximations are then made to reduce the problem into a finite-dimensional one, and analytic or numerical results are obtained. One advantage of Floquet theory is that it allows for the inclusion of dissipative processes relatively easily into the analysis. In this Appendix we briefly outline the application of Floquet theory to the problem of LZS interferometry, closely following (Son et al., 2009). More detailed discussions can be found in Grifoni and Hänggi (1998), Chu and Tel'nov (2004) and Son et al. (2009).

From Floquet's theorem we know that, since the Hamiltonian given by Eqs. (1) and (2) is periodic, there exist two solutions to the Schrödinger equation with the property that

$$\psi_j(t) = \mathrm{e}^{-\mathrm{i}\widetilde{\epsilon}_j t} \widetilde{\psi}_j(t) \tag{D.1}$$

and $\widetilde{\psi}_j(t)$ is a periodic function of t with the same period as the Hamiltonian, i.e., $2\pi/\omega$. Furthermore, these two quasi-periodic solutions are orthogonal and form a complete basis. As a result, knowledge of these states and of the quasi-energies $\widetilde{\epsilon}$ allows one to describe the dynamics for any given initial state.

Finding the Floquet states and quasi-energies is typically achieved using Fourier analysis. Writing

$$\widetilde{\psi}_j(t) = \sum_{n=-\infty}^{+\infty} \xi_{j,n} \mathrm{e}^{\mathrm{i} n \omega t}, \tag{D.2}$$

where each $\xi_{j,n} = (\xi_{j,n,+}, \xi_{j,n,-})^T$ is a two-component vector (with components $\xi_{j,n,+}$ and $\xi_{j,n,-}$), and writing the Hamiltonian (C.1) as

$$H(t) = -\frac{\Delta}{2}\sigma_x - \frac{\varepsilon_0}{2}\sigma_z - \frac{A}{4}\sigma_z \left(\mathrm{e}^{\mathrm{i}\omega t} + \mathrm{e}^{-\mathrm{i}\omega t} \right), \tag{D.3}$$

one obtains the following set of equations governing ξ_{jn}:

$$\widetilde{\varepsilon}\xi_{j,n} = \left(-\frac{\Delta}{2}\sigma_x - \frac{\varepsilon_0}{2}\sigma_z + n\omega \right) \xi_{jn} - \frac{A}{4}\sigma_z \xi_{j,n-1} - \frac{A}{2}\sigma_z \xi_{j,n+1}. \tag{D.4}$$

The task is now to find $\xi_{j,n}$ for all values of n (noting that $\xi_{j,n}$ is composed of the components $\xi_{j,n,-}$ and $\xi_{j,n,+}$) and along with them the quasi-energy $\widetilde{\varepsilon}_j$ (note that the above equations apply to both values of j). If one constructs the infinite-dimensional vector $\widetilde{\xi}_j = \{\ldots, \xi_{j,n-1,-}, \xi_{j,n-1,+}, \xi_{j,n,-}, \xi_{j,n,+}, \xi_{j,n+1,-}, \xi_{j,n+1,+}, \ldots\}$, then the above set of equations governing $\xi_{j,n}$ turns into a single eigenvalue problem

$$\widetilde{\varepsilon}_j \widetilde{\xi}_j = H_F \widetilde{\xi}_j \tag{D.5}$$

where

$$H_F = \begin{pmatrix} \ddots & & & & & \\ & -\frac{\varepsilon_0}{2} + (n-1)\omega & -\frac{\Delta}{2} & -\frac{A}{4} & 0 & 0 & 0 \\ & -\frac{\Delta}{2} & \frac{\varepsilon_0}{2} + (n-1)\omega & 0 & \frac{A}{4} & 0 & 0 \\ & -\frac{A}{4} & 0 & -\frac{\varepsilon_0}{2} + n\omega & -\frac{\Delta}{2} & -\frac{A}{4} & 0 \\ & 0 & \frac{A}{4} & -\frac{\Delta}{2} & \frac{\varepsilon_0}{2} + n\omega & 0 & \frac{A}{4} \\ & 0 & 0 & -\frac{A}{4} & 0 & -\frac{\varepsilon_0}{2} + (n+1)\omega & -\frac{\Delta}{2} \\ & 0 & 0 & 0 & \frac{A}{4} & -\frac{\Delta}{2} & \frac{\varepsilon_0}{2} + (n+1)\omega \\ & & & & & & \ddots \end{pmatrix}. \tag{D.6}$$

This eigenvalue problem has an infinite number of solutions, even though we started by looking for only two solutions. This issue is resolved by noting that this infinite number of solutions can be divided into two groups, each of which contains an infinite number of equivalent solutions; clearly, if there is a solution to the original Floquet problem with quasi-energy $\widetilde{\varepsilon}$, then essentially the same solution can be re-written such that the quasi-energy is given by $\widetilde{\varepsilon} + n\omega$, with any integer n.

The eigenvalue problem derived above cannot be solved in analytic closed form, and approximations have to be made. It is common to treat Δ as a small parameter in a perturbation-theory-like calculation. Taking $\Delta = 0$, one finds the (unperturbed) eigenvectors (Son et al., 2009)

$$
\widetilde{\xi}_{k,-}^{(0)} :
\begin{cases}
\quad\quad\quad \vdots \\
\xi_{k,-,n+k-1,-} = J_1\left(\dfrac{A}{2\omega}\right) \\
\xi_{k,-,n+k-1,+} = 0 \\
\xi_{k,-,n+k,-} = J_0\left(\dfrac{A}{2\omega}\right) \\
\xi_{k,-,n+k,+} = 0 \\
\xi_{k,-,n+k+1,-} = J_1\left(\dfrac{A}{2\omega}\right) \\
\xi_{k,-,n+k+1,+} = 0 \\
\quad\quad\quad \vdots
\end{cases}
\quad\quad
\widetilde{\xi}_{k,+}^{(0)} :
\begin{cases}
\quad\quad\quad \vdots \\
\xi_{k,+,n+k-1,-} = 0 \\
\xi_{k,+,n+k-1,+} = J_1\left(-\dfrac{A}{2\omega}\right) \\
\xi_{k,+,n+k,-} = 0 \\
\xi_{k,+,n+k,+} = J_0\left(-\dfrac{A}{2\omega}\right) \\
\xi_{k,+,n+k+1,-} = 0 \\
\xi_{k,+,n+k+1,+} = J_1\left(-\dfrac{A}{2\omega}\right) \\
\quad\quad\quad \vdots
\end{cases}
,
$$

with quasienergies $\widetilde{\varepsilon}_{k,\pm} = \pm\varepsilon_0/2 - k\omega$ (note that the above eigenvectors are normalized to unity). When two quasienergies are almost equal (specifically $\widetilde{\varepsilon}_{0,-}$ and $\widetilde{\varepsilon}_{k,+}$), and assuming that Δ/ω is small, all others are far off resonance from these two, one can make a rotating-wave approximation and construct an effective two-level problem that involves the two respective Floquet states. Using the relation

$$
\sum_{n=-\infty}^{\infty} J_n(x)J_{k-n}(x) = J_k(2x), \tag{D.7}
$$

one can calculate the effective coupling strength between the two relevant states. The resulting 2×2 effective Hamiltonian is given by

$$
H_{F,RWA} = \frac{1}{2}
\begin{pmatrix}
-\varepsilon_0 & -\Delta J_{-k}\,(A/\omega) \\
-\Delta J_{-k}\,(A/\omega) & \varepsilon_0 - 2k\omega
\end{pmatrix}. \tag{D.8}
$$

Using this effective Hamiltonian, it is now straightforward to find the Floquet states and quasi-energies. The separation between the quasienergies on resonance (i.e., when $\varepsilon_0 = k\omega$) is given by $|\Delta J_k(A/\omega)|$ and determines the oscillation frequency between the two states of the TLS, in clear analogy to the RWA calculation of Appendix C. One can proceed with the calculation in order to obtain more accurate approximations to the Floquet states and quasienergies (Son et al., 2009), but we shall not do this here.

In this Appendix we have re-derived results that we had already derived using the adiabatic-impulse model and the RWA. The use of Floquet theory in this context can therefore be seen as just an alternative approach that can be used to obtain results that can be obtained using other methods. One advantage that the Floquet approach has over the adiabatic-impulse model and the RWA is that decoherence can be introduced into the problem in the Floquet approach following a standard formalism (Grifoni and Hänggi, 1998), whereas the Bloch equations that we have used in Sec. II can be seen as a phenomenological approach to including decoherence in the theoretical analysis. The question of the effects of decoherence on LZS interferometry in the Floquet approach is currently under study (Hausinger and Grifoni, 2010).

Appendix E. Dressed-state picture: quantized driving field

In all our discussion above, we have treated the driving field as an externally applied, classical driving signal. An alternative theoretical approach that can be used to study the problem of a driven quantum system treats the driving field quantum mechanically. The quantum system under study is then enlarged from simply a two-level system to a two-level system and a harmonic oscillator that can have any number of excitations (i.e., photons). As in the Floquet-theory approach, a major advantage that justifies the expansion of the Hilbert space is the simplification associated with turning the time-dependent Hamiltonian into a time-independent one. In fact, the algebra encountered in the Floquet-theory calculation is identical to the one encountered in the dressed-state analysis. The difference between these two approaches is therefore simply the physical interpretation of the mechanisms at play during the system dynamics.

The equivalence between the Floquet approach and the dressed-state approach can be seen by considering the Hamiltonian of the dressed-state picture:

$$
H = -\frac{\Delta}{2}\sigma_x - \frac{\varepsilon_0}{2}\sigma_z + \omega a^\dagger a - \frac{A}{2}\sigma_z\left(a + a^\dagger\right), \tag{E.1}
$$

where a and $a^\dagger$ are the annihilation and creation operators for photons in the electromagnetic field. When written in matrix form, the above Hamiltonian is given by Eq. (D.6) derived in the Floquet approach. More detailed studies of the dressed-state picture can be found in Liu et al. (2006), Greenberg (2007), Wilson et al. (2007) and Wilson et al. (2010).

References

Abragam, A., 1961. The Principles of Nuclear Magnetism. Clarendon, Oxford.
Amin, M.H.S., 2009. Phys. Rev. Lett. 102, 122001.
Ankerhold, J., Grabert, H., 2003. Phys. Rev. Lett. 91, 016803.
Ao, P., Rammer, J., 1991. Phys. Rev. B 43, 5397.
Aravind, P.K., Hirschfelder, J.O., 1984. J. Phys. Chem. 88, 4788.
Arbo, D.G., Ishikawa, K.L., Schiessl, K., Persson, E., Bugdorfer, J., 2010. Phys. Rev. A 81, 021403(R).
Ashhab, S., Johansson, J.R., Nori, F., 2006. Phys. Rev. A 74, 052330.
Ashhab, S., Johansson, J.R., Zagoskin, A.M., Nori, F., 2007. Phys. Rev. A 75, 063414.
Ashhab, S., Johansson, J.R., Zagoskin, A.M., Nori, F., 2009. New. J. Phys. 11, 023030.
Astafiev, O., Inomata, K., Niskanen, A.O., Yamamoto, T., Pashkin, Yu., Nakamura, Y., Tsai, J.S., 2007. Nature 449, 588.
Autler, S.H., Townes, C.F., 1955. Phys. Rev. 100, 703.
Averbukh, I.Sh., Perel'man, I.F., 1985. Sov. Phys. JETP 61, 665.
Banerjee, A., Yakovenko, V.M., 2008. Phys. Rev. B 78, 125404.
Barone, S.R., Narcowich, M.A., Narcowich, F.J., 1977. Phys. Rev. A 15, 1109.
Baruch, M.C., Gallagher, T.F., 1992. Phys. Rev. Lett. 68, 3515.
Benderskii, V.A., Vetoshkin, E.V., Kats, E.I., 2003. JETP 97, 232.
Berns, D.M., Oliver, W.D., Valenzuela, S.O., Shytov, A.V., Berggren, K.K., Levitov, L.S., Orlando, T.P., 2006. Phys. Rev. Lett. 97, 150502.
Berns, D.M., Rudner, M.S., Valenzuela, S.O., Berggren, K.K., Oliver, W.D., Levitov, L.S., Orlando, T.P., 2008. Nature 455, 51.
Bishop, L.S., Chow, J.M., Koch, J., Houck, A.A., Devoret, M.H., Thuneberg, E., Girvin, S.M., Schoelkopf, R.J., 2009. Nature Phys. 5, 105.
Burkard, G., 2010. Science 327, 651.
Bychkov, Yu.A., Dykhne, A.M., 1970. Sov. Phys. JETP 31, 928.
Bylander, J., Rudner, M.S., Shytov, A.V., Valenzuela, S.O., Berns, D.M., Berggren, K.K., Levitov, L.S., Oliver, W.D., 2009. Phys. Rev. B 80, 220506.
Calero, C., Chudnovsky, E.M., Garanin, D.A., 2005. Phys. Rev. B 72, 024409.
Child, M.S., 1974. Molecular Collision Theory. Academic Press, London.
Chu, S.-I., Tel'nov, D.A., 2004. Phys. Rep. 390, 1.
Clarke, J., Wilhelm, F.K., 2008. Nature 453, 1031.
Coffey Jr., D., Lorents, D.C., Smith, F.T., 1969. Phys. Rev. 187, 201.
Cooper, B.K., Yakovenko, V.M., 2006. Phys. Rev. Lett. 96, 037001.
Damski, B., 2005. Phys. Rev. Lett. 95, 035701.
Damski, B., Zurek, W.H., 2006. Phys. Rev. A 73, 063405.
Delone, N.B., Krainov, V.P., 1985. Atoms in Strong Light Fields. In: Springer Series in Chemical Physics, vol. 28. Springer-Verlag, Berlin.
Delos, J.B., Thorson, W.R., 1972. Phys. Rev. A 6, 728.
Devoret, M.H., Martinis, J.M., 2004. Quantum Inf. Process. 3, 163.
Di Giacomo, F., Nikitin, E., 2005. Sov. Phys. Uspekhi 48, 515.
Dutta, S.K., Strauch, F.W., Lewis, R.M., Mitra, K., Paik, H., Palomaki, T.A., Tiesinga, E., Anderson, J.R., Dragt, A.J., Lobb, C.J., Wellstood, F.C., 2008. Phys. Rev. B 78, 104510.
Duty, T., Johansson, G., Bladh, K., Gunnarsson, D., Wilson, C.M., Delsing, P., 2005. Phys. Rev. Lett. 95, 206807.
Dziarmaga, J., 2009. arXiv:0912.4034.
Eckel, J., Reina, J.H., Thorwart, M., 2009. New J. Phys. 11, 085001.
Farhi, E., Goldstone, J., Gutmann, S., Lapan, J., Lundgren, A., Preda, D., 2001. Science 292, 472.
Fink, J.M., Baur, M., Bianchetti, R., Filipp, S., Göppl, M., Leek, P.J., Steffen, L., Blais, A., Wallraff, A., 2009. Phys. Scr. T137, 014013.
Földi, P., Benedict, M.G., Milton Pereira Jr., J., Peeters, F.M., 2007. Phys. Rev. B 75, 104430.
Földi, P., Benedict, M.G., Peeters, F.M., 2008. Phys. Rev. B 77, 013406.
Førre, M., 2004. Phys. Rev. A 70, 013406.
Frasca, M., 2003. Ann. Phys. 306, 193.
Fregenal, D., Horsdal-Pedersen, E., Madsen, L.B., Førre, M., Hansen, J.P., Ostrovsky, V.N., 2004. Phys. Rev. A 69, 031401.
Fuchs, G.D., Dobrovitski, V.V., Toyli, D.M., Heremans, F.J., Awschalom, D.D., 2009. Science 326, 1520.
Gaitan, F., 2003. Phys. Rev. A 68, 052314.
Gallagher, T., 1994. Rydberg Atoms. Cambridge University Press, Cambridge.
Garanin, D.A., 2004. Phys. Rev. B 70, 212403.
Garanin, D.A., Neb, R., Schilling, R., 2008. Phys. Rev. B 78, 094405.
Garraway, B.M., Vitanov, N.V., 1997. Phys. Rev. A 55, 4418.
Gorelik, L.Y., Lundin, N.I., Shumeiko, V.S., Shekhter, R.I., Jonson, M., 1998. Phys. Rev. Lett. 81, 2538.
Goswami, D., 2003. Phys. Rep. 374, 385.
Gradshteyn, I.S., Ryzhik, I.M., 1994. Table of Integrals, Series, and Products. Academic Press, New York.
Grajcar, M., Izmalkov, A., Il'ichev, E., 2005. Phys. Rev. B 71, 144501.
Greenberg, Ya.S., Izmalkov, A., Grajcar, M., Il'ichev, E., Krech, W., Meyer, H.-G., Amin, M.H.S., Maassen van den Brink, A., 2002. Phys. Rev. B 66, 214525.
Greenberg, Ya.S., 2007. Phys. Rev. B 76, 104520.
Grifoni, M., Hänggi, P., 1998. Phys. Rep. 304, 229.
Grossmann, F., Dittrich, T., Jung, P., Hänggi, P., 1991a. Phys. Rev. Lett. 67, 516.
Grossmann, F., Jung, P., Dittrich, T., Hänggi, P., 1991b. Z. Physik B 84, 315.
Grossmann, F., Hänggi, P., 1992. Europhys. Lett. 18, 571.
Hausinger, J., Grifoni, M., 2010. Phys. Rev. A 81, 022117.
Heinrich, G., Harris, J.G.E., Marquardt, F., 2010. Phys. Rev. A 81, 011801.
Henry, C.H., Lang, D.V., 1977. Phys. Rev. B 15, 989.
Ho, T.-S., Hung, S.-H., Chen, H.-T., Chu, S.-I., 2009. Phys. Rev. B 79, 235323.
Il'ichev, E., van der Ploeg, S.H.W., Grajcar, M., Meyer, H.-G., 2009. Quantum Inf. Process. 8, 133.
Il'ichev, E., Shevchenko, S.N., van der Ploeg, S.H.W., Grajcar, M., Temchenko, E.A., Omelyanchouk, A.N., Meyer, H.-G., 2010. Phys. Rev. B 81, 012506.
Irish, E.K., Schwab, K.C., 2003. Phys. Rev. B 68, 155311.
Ithier, G., Collin, E., Joyez, P., Vion, D., Esteve, D., Ankerhold, J., Grabert, H., 2005. Phys. Rev. Lett. 94, 057004.
Izmalkov, A., Grajcar, M., Il'ichev, E., Oukhanski, N., Wagner, Th., Meyer, H.-G., Krech, W., Amin, M.H.S., Maassen van den Brink, A., Zagoskin, A.M., 2004. Europhys. Lett. 65, 844.

Izmalkov, A., van der Ploeg, S.H.W., Shevchenko, S.N., Grajcar, M., Il'ichev, E., Hübner, U., Omelyanchouk, A.N., Meyer, H.-G., 2008. Phys. Rev. Lett. 101, 017003.
Ji, Y., Chung, Y., Sprinzak, D., Heiblum, M., Mahalu, D., Shtrikman, H., 2003. Nature 422, 415.
Johansson, J., Amin, M.H.S., Berkley, A.J., Bunyk, P., Choi, V., Harris, R., Johnson, M.W., Lanting, T.M., Lloyd, S., Rose, G., 2009. Phys. Rev. B 80, 012507.
Kayanuma, Y., 1994. Phys. Rev. A 50, 843.
Kayanuma, Y., 1997. Phys. Rev. A 55, R2495.
Kayanuma, Y., Saito, K., 2008. Phys. Rev. A 77, 010101(R).
Krainov, V.P., Yakovlev, V.P., 1980. Sov. Phys. JETP 51, 1104.
Kral, P., Thanopulos, I., Shapiro, M., 2007. Rev. Mod. Phys. 79, 53.
LaHaye, M.D., Suh, J., Echternach, P.M., Schwab, K.C., Roukes, M.L., 2009. Nature 459, 960.
Landau, L., 1932a. Phys. Z. Sowjetunion 1, 88.
Landau, L., 1932b. Phys. Z. Sowjetunion 2, 46.
Landau, L.D., Lifshitz, E.M., 1977. Quantum Mechanics: Non-Relativistic Theory. Pergamon Press, Oxford.
Leggett, A.J., Chakravarty, S., Dorsey, A.T., Fisher, M.P.A., Garg, A., Zwerger, W., 1987. Rev. Mod. Phys. 59, 1.
Li, R., Hoover, M., Gaitan, F., 2009. Quantum Inf. Comput. 9, 290.
Liao, J.-Q., Gong, Z.R., Zhou, L., Liu, Y.X., Sun, C.P., Nori, F., 2010. Phys. Rev. A 81, 042304. arXiv:0909.2748.
Liu, Y.X., Sun, C.P., Nori, F., 2006. Phys. Rev. A 74, 052321.
Lopez-Castillo, J.-M., Filali-Mouhim, A., Jay-Gerin, J.-P., 1992. J. Chem. Phys. 97, 1905.
Maeda, H., Gurian, J.H., Norum, D.V.L., Gallagher, T.F., 2006. Phys. Rev. Lett. 96, 073002.
Majorana, E., 1932. Nuovo Cimento 9, 43.
Makhlin, Yu., Schön, G., Shnirman, A., 2001. Rev. Mod. Phys. 73, 357.
Mark, M., Kraemer, T., Waldburger, P., Herbig, J., Chin, C., Nägerl, H.-C., Grimm, R., 2007a. Phys. Rev. Lett. 99, 113201.
Mark, M., Ferlaino, F., Knoop, S., Danzl, J.G., Kraemer, T., Chin, C., Nägerl, H.-C., Grimm, R., 2007b. Phys. Rev. A 76, 042514.
Marzlin, K.-P., Sanders, B.C., 2004. Phys. Rev. Lett. 93, 160408.
McDermott, R., 2009. IEEE Trans. Appl. Supercond 19, 2.
Mukherjee, V., Dutta, A., 2009. J. Stat. Mech. P05005.
Mullen, K., Ben-Jacob, E., Gefen, Yu., Schuss, Z., 1989. Phys. Rev. Lett. 62, 2543.
Nagaya, K., Zhu, C., Lin, S.H., 2007. J. Chem. Phys. 127, 094304.
Nakamura, Y., Pashkin, Yu.A., Tsai, J.S., 2001. Phys. Rev. Lett. 87, 246601.
Nalbach, P., Thorwart, M., 2009. Phys. Rev. Lett. 103, 220401.
Nikitin, E.E., 1996. In: Drake, G.W.F. (Ed.), Atomic, Molecular and Optical Physics Handbook. Americal Institute of Physics, Woodbury, NY, p. 561.
Nikitin, E.E., Ovchinnikova, M.Ya., 1972. Sov. Phys. Uspekhi 14, 394.
Nikitin, E.E., Umanskii, S.Ya., 1984. Theory of Slow Atomic Collisions. Springer, Heidelberg.
Oh, S., Huang, Z., Peskin, U., Kais, S., 2008. Phys. Rev. A 78, 062106.
Oliver, W.D., Valenzuela, S.O., 2009. Quantum Inf. Process. 8, 261.
Oliver, W.D., Yu, Ya., Lee, J.C., Berggren, K.K., Levitov, L.S., Orlando, T.P., 2005. Science 310, 1653.
Paila, A., Tuorila, J., Sillanpää, M., Gunnarsson, D., Sarkar, J., Makhlin, Yu., Thuneberg, E., Hakonen, P., 2009. Quantum Inf. Process. 8, 245.
Pegg, D.T., Series, G.W., 1973. Proc. R. Soc. A 332, 281.
Persson, F., Wilson, C.M., Sandberg, M., Johansson, G., Delsing, P., 2010. Nano Lett. 10, 953.
Petta, J.R., Lu, H., Gossard, A.C., 2010. Science 327, 669.
Pezze, L., Smerzi, A., Khoury, G., Hodelin, J.F., Bouwmeester, D., 2007. Phys. Rev. Lett. 99, 223602.
Pokrovsky, V.L., Sinitsyn, N.A., 2002. Phys. Rev. B 65, 153105.
Pokrovsky, V.L., Sinitsyn, N.A., 2004. Phys. Rev. B 69, 104414.
Rabi, I.I., 1937. Phys. Rev. 51, 652.
Ribeiro, H., Burkard, G., 2009. Phys. Rev. Lett. 102, 216802.
Ribeiro, H., Petta, J.R., Burkard, G., 2010. arXiv:1002.4630.
Ritus, V.I., 1967. Sov. Phys. JETP 24, 1041.
Rodrigues, D.A., Imbers, J., Armour, A.D., 2007a. Phys. Rev. Lett. 98, 067204.
Rodrigues, D.A., Imbers, J., Harvey, T.J., Armour, A.D., 2007b. New J. Phys. 9, 84.
Rotvig, J., Jauho, A.P., Smith, H., 1995. Phys. Rev. Lett. 74, 1831.
Rotvig, J., Jauho, A.P., Smith, H., 1996. Phys. Rev. B 54, 17691.
Rudner, M.S., Shytov, A.V., Levitov, L.S., Berns, D.M., Oliver, W.D., Valenzuela, S.O., Orlando, T.P., 2008. Phys. Rev. Lett. 101, 190502.
Saito, S., Thorwart, M., Tanaka, H., Ueda, M., Nakano, H., Semba, K., Takayanagi, H., 2004. Phys. Rev. Lett. 93, 037001.
Saito, K., Kayanuma, Y., 2002. Phys. Rev. A 65, 033407.
Saito, K., Wubs, M., Kohler, S., Kayanuma, Y., Hänggi, P., 2007. Phys. Rev. B 75, 214308.
Sambe, H., 1973. Phys. Rev. A 7, 2203.
Sarandy, M.S., Wu, L.-A., Lidar, D.A., 2004. Quantum Inf. Process. 3, 331.
Shevchenko, S.N., Kiyko, A.S., Omelyanchouk, A.N., Krech, W., 2005. Low Temp. Phys. 31, 569.
Shevchenko, S.N., Omelyanchouk, A.N., 2006. Low Temp. Phys. 32, 973.
Shevchenko, S.N., van der Ploeg, S.H.W., Grajcar, M., Il'ichev, E., Omelyanchouk, A.N., Meyer, H.-G., 2008. Phys. Rev. B 78, 174527.
Shimshoni, E., Gefen, Y., 1991. Ann. Phys. 210, 16.
Shirley, J.H., 1965. Phys. Rev. 138, B979.
Shnyrkov, V.I., Wagner, Th., Born, D., Shevchenko, S.N., Krech, W., Omelyanchouk, A.N., Il'ichev, E., Meyer, H.-G., 2006. Phys. Rev. B 73, 024506.
Shnyrkov, V.I., Born, D., Soroka, A.A., Krech, W., 2009. Phys. Rev. B 79, 184522.
Shytov, A.V., Ivanov, D.A., Feigel'man, M.V., 2003. Eur. Phys. J. B 36, 263.
Shytov, A.V., 2004. Phys. Rev. A 70, 052708.
Sillanpää, M., Lehtinen, T., Paila, A., Makhlin, Yu., Roschier, L., Hakonen, P., 2005. Phys. Rev. Lett. 95, 206806.
Sillanpää, M., Lehtinen, T., Paila, A., Makhlin, Yu., Hakonen, P., 2006. Phys. Rev. Lett. 96, 187002.
Sillanpää, M., Lehtinen, T., Paila, A., Makhlin, Yu., Hakonen, P., 2007. J. Low Temp. Phys. 146, 253.
Son, S.-K., Han, S., Chu, S.-I., 2009. Phys. Rev. A 79, 032301.
Stückelberg, E.C.G., 1932. Helv. Phys. Acta 5, 369.
Sun, G., Chen, J., Ji, Z., Xu, W., Kang, L., Wu, P., Dong, N., Mao, G., Yu, Y., Xing, D., 2006. Appl. Phys. Lett. 89, 082516.
Sun, G., Wen, X., Wang, Y., Cong, S., Chen, J., Kang, L., Xu, W., Yu, Y., Han, S., Wu, P., 2009. Appl. Phys. Lett. 94, 102502.
Teranishi, Y., Nakamura, H., 1998. Phys. Rev. Lett. 81, 2032.
Thorwart, M., Grifoni, M., Hänggi, P., 2000. Phys. Rev. Lett. 85, 860.
Thorwart, M., Grifoni, M., Hänggi, P., 2001. Ann. Phys. 293, 15.
Tong, D.M., Singh, K., Kwek, L.C., Oh, C.H., 2005. Phys. Rev. Lett. 95, 110407.
Tong, D.M., Singh, K., Kwek, L.C., Oh, C.H., 2007. Phys. Rev. Lett. 98, 150402.
Tornes, I., Stroud, D., 2008. Phys. Rev. B 77, 224513.
van Ditzhuijzen, C.S.E., Tauschinsky, A., van Linden van den Heuvell, H.B., 2009. Phys. Rev. A 80, 063407.
Vitanov, N.V., Garraway, B.M., 1996. Phys. Rev. A 53, 4288.

Vitanov, N.V., 1999. Phys. Rev. A 59, 988.
Vitanov, N.V., Halfmann, Th., Shore, B.W., Bergmann, K., 2001. Annu. Rev. Phys. Chem. 52, 763.
Vitanov, N.V., Yatsenko, L.P., Bergmann, K., 2003. Phys. Rev. A 68, 043401.
Wallraff, A., Duty, T., Lukashenko, A., Ustinov, A.V., 2003. Phys. Rev. Lett. 90, 037003.
Wang, Y., Cong, S., Wen, X., Pan, C., Sun, G., Chen, J., Kang, L., Xu, W., Yu, Y., Wu, P., 2010. Phys. Rev. B 81, 144505.
Wei, L.F., Johansson, J.R., Cen, L.X., Ashhab, S., Nori, F., 2008. Phys. Rev. Lett. 100, 113601.
Wen, X., Yu, Y., 2009. Phys. Rev. B 79, 094529.
Wendin, G., Shumeiko, V.S., 2007. Low Temp. Phys. 33, 724.
Wernsdorfer, W., Sessoli, R., Caneshi, A., Gatteschi, D., Cornia, A., 2000. Europhys. Lett. 50, 552.
Wilhelm, F.K., 2008. Nature 455, 41.
Wilson, C.M., Duty, T., Persson, F., Sandberg, M., Johansson, G., Delsing, P., 2007. Phys. Rev. Lett. 98, 257003.
Wilson, C.M., Johansson, G., Duty, T., Persson, F., Sandberg, M., Delsing, P., 2010. Phys. Rev. B 81, 024520.
Wittig, C., 2005. J. Phys. Chem. B 109, 8428.
Wubs, M., Saito, K., Kohler, S., Kayanuma, Y., Hänggi, P., 2005. New J. Phys. 7, 218.
Wubs, M., Saito, K., Kohler, S., Hänggi, P., Kayanuma, Y., 2006. Phys. Rev. Lett. 97, 200404.
Wubs, M., 2010. doi:10.1016/j.chemphys.2010.03.003, arXiv:1001.4614.
Yoakum, S., Sirko, L., Koch, P.M., 1992. Phys. Rev. Lett. 69, 1919.
You, J.Q., Nori, F., 2005. Physics Today 58 (11), 42.
Yu, Y., Oliver, W.D., Lee, J.C., Berggren, K.K., Levitov, L.S., Orlando, T.P., 2005. eprint arXiv:cond-mat/0508587.
Zagoskin, A., Blais, A., 2007. Phys. Canada 63, 215.
Zenesini, A., Lignier, H., Tayebirad, G., Radogostowicz, J., Ciampini, D., Mannella, R., Wimberger, S., Morsch, O., Arimondo, E., 2009. Phys. Rev. Lett. 103, 090403.
Zel'dovich, Ya.B., 1973. Sov. Phys. Usp. 16, 427.
Zener, C., 1932. Proc. R. Soc. Lond. A 137, 696.
Zhang, Q., Hänggi, P., Gong, J.B., 2008a. Phys. Rev. A 77, 053607.
Zhang, Q., Hänggi, P., Gong, J.B., 2008b. New J. Phys. 10, 073008.
Zhou, L., Gong, Z.R., Liu, Y.X., Sun, C.P., Nori, F., 2008a. Phys. Rev. Lett. 101, 100501.
Zhou, L., Dong, H., Liu, Y.X., Sun, C.P., Nori, F., 2008b. Phys. Rev. A 78, 063827.
Zhu, C., Teranishi, Y., Nakamura, H., 2001. Adv. Chem. Phys. 117, 127.
Zueco, D., Hänggi, P., Kohler, S., 2008. New J. Phys. 10, 115012.
Zurek, W.H., 1996. Phys. Rep. 276, 177.
Zwanziger, J.W., Werner-Zwanziger, U., Gaitan, F., 2003. Chem. Phys. Lett. 375, 429.